Using novel geophysical techniques to relate surface coal mining fill characteristics to effluent stream water quality

OSMRE Cooperative Agreement Number: # S16AC20076
Final Report

Reporting Period: 10/1/2016 – 12/31/2018
Principal Authors:

Erich Hester (Lead Investigator)
Associate Professor, Civil and Environmental Engineering
Virginia Tech. Blacksburg, VA 24061
540-231-9758. ehester@vt.edu

Carl Zipper
Professor, School of Plant and Environmental Sciences
Virginia Tech. Blacksburg, VA 24061
540-231-9782. czip@vt.edu

Tom Burbey
Professor, Geosciences
Virginia Tech. Blacksburg, VA 24061
540-231-6696. tjburbey@vt.edu

Katie Little
Graduate Research Assistant, Civil and Environmental Engineering
Virginia Tech. Blacksburg, VA 24061

Joseph Buckwalter
Research Associate
Virginia Tech. Blacksburg, VA 24061

Report Date: April 2019

OSMRE Award Number: # S16AC20076

Submitting Organization: Virginia Polytechnic Institute and State University
Office of Sponsored Programs
North End Center
300 Turner Street NW
Suite 4200 (MC 0170)
Blacksburg, Virginia 24061

DISCLAIMER

ABSTRACT

Surface coal mining in Appalachia increases total dissolved solids (TDS) in mine effluents, affecting aquatic ecology throughout central Appalachia, with challenges for mine permitting. Yet the causal link between mine characteristics and variations in mine-discharge TDS concentrations remains unclear. Knowledge of the hydrologic flowpaths through mine-spoil fills is needed to determine where, when, and how much TDS is acquired by infiltrating waters and delivered to streams. We used the geophysical technique electrical resistivity imaging (ERI) to map hydrologic flowpaths through a series of valley fills, which allows a far more complete understanding of valley-fill hydrologic response than possible with conventional approaches. The fills are known as Office Fill, End Fill, Bearwallow, and Barton Hollow. Barton Hollow is an experimental fill designed to reduce TDS effluent, while the remaining fills used conventional construction. We used ERI surveys in dry conditions to reveal subsurface geology/lithology and during artificial rainfall experiments to reveal stormflow hydrology. We attempted to relate the hydrologic information learned from ERI to controlling factors such as fill construction and reclamation approaches, age of mining, and size of mined watersheds. We also verified our ERI interpretations with a series of strategically executed hydrogeologic investigations including borings, excavation, and fluorescent dye tracers. Our results confirmed the value of ERI as a noninvasive tool for hydrogeologic analysis of valley fills. We found considerable variability among conventional fills in terms of subsurface structure and infiltration hydrology. Shallow moisture retention in fine spoils above larger rocks with void spaces were common in conventional loose-dump valley fills. Deep preferential infiltration flowpaths are a common feature of these conventional fills, where transit velocities are much higher than in undisturbed lands. By contrast, the experimental design of Barton Hollow fill, which helped control infiltration to the deep bulk fill, appeared to yield improved effluent water quality. Our analysis of the relationship between hydrologic response and fill construction and reclamation approaches did not yield statistically significant results. Yet our interpretations of ERI results were successfully verified by traditional methods, including boring and downhole camera, and use of fluorescent dye tracer followed by shallow excavation.

LIST OF GRAPHICAL MATERIALS

1. INTRODUCTION

1.1 Background

Surface coal mining in Appalachia entails blasting of consolidated bedrock which creates smaller rock fragments which are placed in fills. These occur both within the original mined area (e.g., highwall fill) and in adjacent valleys (valley fills). This rock fragmentation, together with the manner in which those fragmented rocks are placed in fills during landscape reconstruction, alters hydrologic flowpaths and water storage within the fills. The mechanical compaction of fill surfaces, together with "hydrocompaction" of fine rock fragments and rock flour, can create relatively impervious surfaces that can increase peak storm flows in streams draining mined watersheds (Simmons et al. 2008). In addition, the reduced evapotranspiration that results when native forests are replaced with grass cover can simultaneously increase baseflows in those streams (Miller and Zegre 2014, Evans et al. 2015).

The fragmentation of rock exposes fresh surfaces to the elements, which causes the rock surfaces to weather at greatly increased rates, thus releasing dissolved minerals. Appalachian surface coal mining therefore also influences the quality of waters in streams draining mined watersheds. In particular, total dissolved solids (TDS) is commonly elevated, and aquatic communities are commonly altered relative to a reference condition (Hartman et al. 2005, Pond et al. 2008, Griffith et al. 2012, Cormier et al. 2013, Pond et al. 2014, Timpano et al. 2015). The net effect of fill construction is that both geologic and hydrologic alterations interact to induce elevation in TDS of discharged waters. This has caused mine permitting to become more difficult, which is of concern to mining companies. Yet great variability is observed among mined watersheds in terms of TDS in effluent streams (Merricks et al. 2007, Mack et al. 2013, Evans et al. 2014). Differences in the geologic alteration, such as rock placement and fill construction processes, and related variables such as fill reclamation techniques and fill age are expected to cause many of these variations in fill hydrology and TDS release.

Yet the relationship between reconstructed landscape geology, hydrology, and TDS remains unclear. Water may minimally infiltrate mine-spoil fills due to a highly compacted surface layer (Simmons et al. 2008), or may infiltrate more rapidly (Guebert and Gardner 2001, Greer et al. 2017). Within the fill, water may move along preferential flow paths sometimes referred to as "pseudokarst" (Caruccio and Geidel 1984, Hawkins and Aljoe 1992), or it may saturate fine-textured materials. The latter is expected to cause greater TDS release than preferential flows due to greater time for water-rock interactions that lead to mineral leaching. Yet prior to this project, these processes had only been surmised rather than directly observed. Prior hydrologic measurements generally treated fills as "black boxes" by measuring water infiltrating at the surface or emerging as stream flow at the bottom (Hawkins and Aljoe 1992, Hawkins 1998, Wunsch et al. 1999, Hawkins 2004).

Understanding TDS generation requires understanding flow process that occur within the interior of fills. This can show where in the fills infiltrating water slows down enough (i.e. is "stored") for the kinetics of mineral leaching to substantially occur. This in turn allows association of those locations with the causes of their creation such as compaction surfaces generated during lift creation. This ultimately could allow future fills to be constructed in ways that do not create such enhanced opportunities for leaching. Furthermore, coal mining overburden varies widely in TDS-generating potential, such that soils, saprolite, and shallower bedrock tend to have relatively low TDS-generation potential due to prior weathering, deeper

bedrock tends to have higher TDS-generation potential due to less prior weathering, and TDS-generation potentials of deeper bedrock ("unweathered spoils") varies among spoil materials (Agouridis et al. 2012, Daniels et al. 2013, Daniels et al. 2015, Orndorff et al. 2015). Improved understanding of how infiltrating water flows through valley fills can allow future fills to be built in ways that isolate high-TDS generating materials from hydrologic processes (Zipper et al. 2015). This knowledge will also allow more informed monitoring and permitting of existing mines. Yet traditional hydrologic techniques such as infiltrometers, stream hydrology or TDS measurements, and groundwater wells provide only limited "illumination" of fill interiors. More holistic approaches are needed.

Our ability to link variables such as fill construction or reclamation techniques with TDS outcomes is underpinned by the hydrology of mine-spoil fills and other mined landscapes because it is those hydrologic flowpaths through mined areas that control where, when, and how much TDS is picked up and delivered to effluent streams. Our knowledge of this hydrology has been limited by use of conventional hydrologic measurement techniques that cannot capture the hydrologic flowpaths that ultimately control TDS generation. Through a preliminary case study conducted prior to this project (Greer et al. 2017), we were able to demonstrate that the geophysical technique electrical resistivity imaging (ERI) can map these hydrologic flowpaths through valley fills and also determine water residence times. Hence, ERI offers opportunity for improved understanding of valley fill hydrology relative to conventional hydrologic techniques.

1.2 Objectives

The overall goal of this project was to determine locations of preferential flowpaths of infiltrating rainwater and water accumulation zones within surface coal mine valley fills, see their variation among different fills including an experimental fill designed to reduce TDS levels in effluent, and link this hydrologic characterization to TDS generation. The specific objectives were to:

1. Map hydrologic flowpaths (i.e. determine their locations) through the interiors of a series of valley fills during precipitation events.
2. Determine the residence times of those flowpaths.
3. Determine how flowpath location and residence time control the contribution of flowpaths to TDS/SC in the effluent stream.
4. Determine how variations in flowpaths, residence times, and therefore contributions to TDS/SC are controlled by factors such as fill age, construction method, and reclamation method.
5. Independently verify hydrologic interpretations of ERI results using complementary hydrogeologic techniques.

1.3 Tasks and Organization of Final Report Document

To address the Objectives listed above in Section 1.2, the following tasks were proposed in the Statement of Work. The methods for, results of, and discussion of results for each of these tasks are listed by Task number in Sections 3 and 4, below.

1. Electrical resistivity imaging (ERI) of valley fills, including preparation for fieldwork, ERI surveys both dry and with artificial rainfall, and ERI data inversion

2. Verification of ERI results, including tracer (rhodamine) in artificial rainfall, monitoring of effluent streams, excavation, and boring(s)
3. Monitoring streams and natural rainfall events, including measuring flow in effluent streams, developing rating curves, measuring precipitation, and measuring stage and electrical specific conductance in effluent streams, application of tracer (rhodamine) during natural storms with monitoring of effluent stream
4. Relating valley fill geology with effluent hydrology and water quality

2. EXECUTIVE SUMMARY

2.1 Introduction

Surface coal mining in Appalachia increases total dissolved solids (TDS) in mine effluents, affecting aquatic ecology throughout central Appalachia, and challenges for mine permitting. TDS levels vary among streams draining mined lands due to differences in factors such as fill age, construction technique, and reclamation method but the causal link between these variables and mine-discharge TDS concentrations remains unclear. The link between fill construction or reclamation techniques and TDS effects is the hydrology of mine-spoil fills and other mined landscapes. Hydrologic flowpaths through mine-spoil fills determine where, when, and how much TDS is acquired by infiltrating waters and delivered to streams. Knowledge of such hydrology has been restrained by use of conventional hydrologic measurement methods that entail point measurement of water quality and quantity inputs and outputs but do not capture the hydrologic fill-interior flowpaths that ultimately determine TDS discharge. Our goal was to use the geophysical technique, electrical resistivity imaging (ERI), to map hydrologic flowpaths through valley fills. This technique enables assessment of fill infiltration and interior flowpaths, and therefore a far more complete understanding of valley-fill hydrologic than is possible using conventional techniques. The specific objectives of the project were to 1) map hydrologic flowpaths through the interiors of a series of valley fills during precipitation events, 2) determine the residence times of those flowpaths, 3) determine how flowpath location and residence time control the contribution of flowpaths to TDS/SC in the effluent streams, 4) determine how variations in flowpaths, residence times, and therefore contributions to TDS/SC are controlled by factors such as fill age, construction method, and reclamation method, and 5) independently verify hydrologic interpretations of ERI results using complementary hydrogeologic techniques.

2.2 Methods

We used ERI to map and determine the residence times of hydrologic flowpaths through the interior of a series of valley fills during precipitation events. The fills are known as Office Fill, End Fill, Bearwallow, and Barton Hollow. Barton Hollow is an experimental fill where low-TDS material was placed in compacted lifts to reduce TDS effluent; the other fills were constructed using conventional loose-dump methods. We used ERI surveys in dry conditions to reveal subsurface geology/lithology and during artificial rainfall experiments to reveal stormflow hydrology. We attempted to relate the hydrologic information learned from ERI to controlling factors such as fill construction and reclamation approaches, age of mining, and size of mined watersheds. We also verified our ERI interpretations with a series of strategically executed hydrogeologic investigations including borings, excavation, and fluorescent dye tracers. These increased our confidence in the ERI results and our associated conclusions.

2.3 Results

Objective 1. We found significant variation in subsurface structure among fills. Barton Hollow had a relatively small range of resistivity compared to the conventional fills, suggesting more consistent structure. We observed fewer deep accumulation zones at Barton Hollow, suggesting the internal structure helps keep infiltration shallow.

Objective 2. Based on the identified accumulation zones, we estimated an average infiltration flowpath velocity of $\geq$5.1 m/h or $\geq$0.14 cm/s. These velocities indicate faster infiltration than that observed on many natural lands.

Objective 3. Neither the fluorescent rhodamine tracer exercise with artificial rainfall nor that with natural rainfall provided data that were useful in interpreting valley fill hydrology because of greater sorption of tracer to fill soils than expected and rhodamine sensor interference from turbidity. Yet this experience provided lessons learned that can inform future efforts.

Objective 4. Baseflow at Office Fill was higher and less variable than at End Fill, Barton Hollow, and Bearwallow. Average SC was lowest at Barton Hollow, likely due to experimental fill construction practices. Regressions of quantifiable fill (such as fill age, construction method, and reclamation method) and flowpath properties (such as length, transit time, velocity) did not reveal any statistically significant relationships.

Objective 5. Observations from soil pits and infiltration studies successfully corroborated ERI interpretations. At Office Fill and End Fill, soil pits revealed voids between rocks that were consistent with preferential flow patterns observed via ERI. Down-hole video and cores at Office Fill successfully verified ERI interpretations. In particular, smaller rocks with more fines and more moisture retention were found near the surface of the valley fill and larger rocks with larger voids and less moisture retention were found at depth.

2.4 Conclusions

This project confirmed the value of ERI as a noninvasive tool for hydrogeologic analysis of valley fills, able to image internal structure under dry conditions and subsurface flowpaths under rainfall. We found considerable variability among conventional loose-dump fills in terms of subsurface structure and infiltration hydrology. Deep preferential infiltration flowpaths are a common feature of conventional loose-dump valley fills, where transit velocities are much higher than in undisturbed lands, confirming the concept of "pseudokarst". By contrast, the experimental design of Barton Hollow fill, where uniform lifts with compaction help control infiltration to the deep bulk fill, appear to yield improved effluent water quality.

Several assessment approaches employed by this project verified our interpretations of ERI tomograms. For example, the boring and downhole camera confirmed finer soil particles at shallow depths that retain moisture overlying larger rocks with void spaces in between at greater depths that do not retain moisture. Additionally, application of fluorescent dye tracer followed by shallow excavation confirmed the presence of preferential flowpaths through the surface layer. While monitoring fluorescent dye in effluent streams was not successful due to sorption of dye by spoil materials and interference of water measurements by turbidity, useful recommendations were made for future efforts.

2.5 Dissemination

Dissemination occurred via 1) a conference presentation at the American Society of Mining and Reclamation conference in June 2018, 2) a peer-reviewed scientific journal article (Hester, E.T., Little, K.L., Buckwalter, J.D., Zipper, C.E., and Burbey, T.J. 2019. Variability of subsurface structure and infiltration hydrology among surface coal mine valley fills. *Science of the Total Environment* 651, 2648-2661), 3) a public archive of the ERI data at www.hydroshare.org/resource/b1d5fd2c2d3e49878d86cb7c2d483d2a, 4) an article in the trade journal Reclamation Matters (Hester E.T., Little, K.L., Buckwalter, J.D., Zipper, C.E., and Burbey, T.J. How infiltration hydrology varies among Appalachian coal-mine valley fills. Reclamation Matters 2019, Spring, p. 37-39), and 5) Kathryn Little's MS Thesis at Virginia Tech.

3. EXPERIMENTAL

This study involved four field sites in southwestern Virginia, which we refer to as Barton Hollow, Office Fill, End Fill, and Bearwallow. They are all valley fills of reclaimed surface coal mines but vary in age, land cover, and size (Figure 3-1, Table 3-1). Our original intent was to monitor two experimental fills and two conventional fills. We were unable to conduct ERI imaging at a second experimental fill, as intended, because it remained under active construction during the full study period. Therefore, a third conventional fill was substituted.

Figure 3-1. Aerial view of the four field sites: (a) Barton Hollow; (b) Office Fill (top left) and End Fill (bottom right); (c) Bearwallow. White solid lines denote the approximate location of fill boundaries. The Bearwallow fill was constructed within a mined landscape and therefore does not have clearly defined perimeter boundaries as do the other three fills. White dashed lines denote the locations of long ERI transects. Red dashed lines denote the locations of short ERI transects with artificial rainfall. Areal map (d) shows the relative locations of the four sites. All views are oriented such that north is up.

Table 3-1. Valley Fill Field Site Properties

Fill	Approximate Time since Revegetation (yr)	Land Cover	Fill Area* (ha)	Watershed Area* (ha)	Mean Effluent Stream SC during Study (µS/cm)
Barton Hollow	2	Long grass with sparse small trees	7	53	1722
Office Fill	9	Dense underbrush, some trees, a few grassy areas	3	42	2540
End Fill	21	Mature forest	2	30	1989
Bearwallow	11	Dense underbrush, some trees, a few grassy areas	15	25	2199

**We estimated valley fill areas using Google Earth imagery and watershed areas using ArcGIS and the 2013 10-meter National Elevation Dataset. For SC, see Figure D-1. Typical SC values for forested, unmined watersheds are <200 µS/cm (Pond et al. 2008, Timpano et al. 2015).*

Office Fill, End Fill, and Bearwallow were all constructed using a conventional loose-dump method, in which material is dumped into the valley from the top of the slope. The largest boulders tend to roll down the slope and gather near the toe of the fill. Finer material comes to rest higher up. Bulldozers then arrange the slope into its final shape. At Bearwallow, a majority of the fill material is hard sandstone which serves as a durable material for the bulk of the fill (C. Stanley, personal communication, January 8, 2018). Office Fill is composed of a variety of materials including durable sandstone but also with some weathered surface material, siltstone, and soft sandstone (personal communication from Paramont Coal personnel). End Fill is very near to Office Fill (~800 meters between fills' toes) and has similar types of fill material. The details of construction for both fills are also unknown.

Barton Hollow was constructed with an experimental structure. The goal of the construction method was to reduce the TDS in the valley's effluent stream. Thus, the fill contained primarily weathered rocks and spoil material that would contribute low levels of TDS. This would be compacted, if possible, a few meters from the surface to help fines settle into a lower-permeability layer. Any remaining higher-TDS material would be placed "high and dry," i.e., higher up the slope in a region farther from the main drains and not prone to flooding, to reduce its contact time with water (Zipper et al. 2015). To accomplish this plan, Barton Hollow was constructed as a series of vertical lifts, approximately 50 feet in thickness, with compacted surfaces, separated by horizontal benches (Figure 3-2).

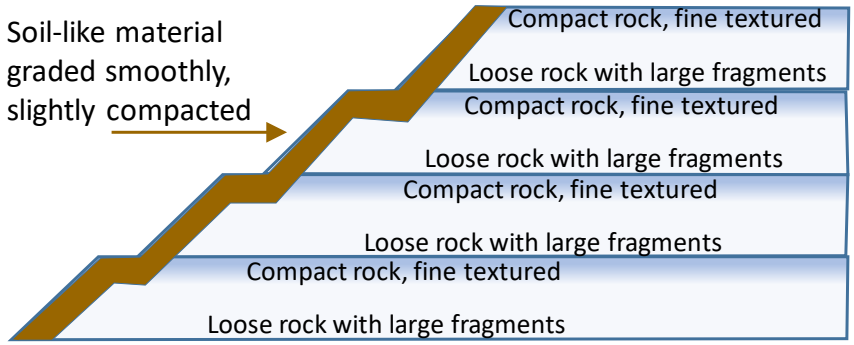

Figure 3-2. Simplified cross-sectional diagram of Barton Hollow's internal structure expected based upon the experimental construction method. Five vertical sections are shown, each approximately 50 feet thick.

The lifts were built separately and sequentially, from the bottom of the fill to the top. However, each individual lift was built from right to left in the diagram. Trucks backed out toward the left, compacting the surface in the process, and dumped material over the edge to extend the lift farther to the left. Rocks naturally segregated over the 50-foot depth of the lift, with larger rocks rolling to the bottom to lodge upon the compacted surface of the lift directly below. To complete each lift, soil-sized material was added on top of the mine spoil on the lift's exposed surface (far left in Figure 3-2) for revegetation. The mine-spoil rock materials placed in the fill were of two types: hard sandstone with boulders, determined to have low-TDS generating properties via procedures described by Orndorff et al. (2015), and weathered rock also with low-TDS generating properties. By contrast, Office Fill and End Fill have a terraced form similar to that of Barton Hollow but were described by mining company personnel as lacking the compacted internal surfaces and separate lifts, while Bearwallow has only one notable horizontal bench within the transect we surveyed and also lacks internal compaction and separate lifts.

3.1 Electrical Resistivity Imaging (ERI) of Valley Fills

3.1.1 Long Dry ERI Surveys

We gathered ERI data at each of the four field sites using a SuperSting R8 resistivity system, consisting of a resistivity meter, switch box, stainless steel electrodes, and various cables, all manufactured by Advanced Geosciences, Inc. (AGI) (Appendix B). We performed one overall linear survey on each fill. These transects covered the entire lengths of End Fill and Office Fill, from toe to crest. At the larger Barton Hollow and Bearwallow fills, the transects covered most but not the entire lengths of the fills due to factors including fill size, equipment limitations, and active roads. The transects ranged from 167 meters to over 400 meters (Table 3-2).

At Barton Hollow, Office Fill, and End Fill, we used all four cables (64 electrodes) available in order to achieve the maximum resolution possible. At Bearwallow, we used 32 electrodes due to bear-induced damage to a cable. Electrode spacing varied among long transect surveys and ranged from 2.65 m to 10.0 m (Table 3-2). We ran an automatic ERI survey with a dipole-dipole array, which provides more reliable data at depth and better resolution of vertical structure changes relative to other arrays (Herman 2001, Seaton and Burbey 2002) while still maintaining a fairly quick survey time of about 33 minutes for a 64-electrode setup and about 8

minutes for a 32-electrode setup. These surveys (Table 3-2) were performed under dry conditions, i.e., it had not rained for over 48 hours.

Table 3-2. Summary of Long Dry ERI Surveys

Date	Fill	Transect Length (m)	Electrode Spacing (m)	Days since Last Rainfall*
06/12/2017	Barton Hollow	422.1	6.7	7
07/12/2017	Office Fill	210	3.33	6
08/25/2017	End Fill	167	2.65	2
10/03/2017	Bearwallow	310	10.0	19

**Figure D-2*

3.1.2 Short Artificial Rainfall ERI Surveys

We also performed a series of surveys on shorter transects near the bottom of each fill slope, typically on the bottommost lift, to monitor rainfall infiltration into the fill. We conducted artificial rainfall sprinkling on short transects to achieve better spatial ERI resolution and due to the impracticalities of pumping water over the entire fill. The short transect usually spanned about one lift, but the location of the top boundary depended on the vertical distance from the pump and the water pressure of the sprinkler flow (Table 3-3).

We again used all 64 electrodes for all of these surveys except at Bearwallow, where we used 32 electrodes due to the broken cable. The setup process for the electrodes, cables, and box was essentially the same as that for the long transects, described above. The electrode spacing was reduced due to the shorter lengths of the transects (Table 3-3), and we also covered all cable connections with plastic wrap and duct tape in order to prevent water damage. Once setup was complete, we again performed a contact resistivity test and adjusted electrodes as necessary before proceeding with the ERI surveys.

The first survey in each series was performed under dry conditions, i.e., after at least 48 hours of no precipitation as measured by the rain gauges on each fill (Figure D-2). Following the dry survey, water was pumped from the bottom of the fill through sprinklers spaced along the transect in order to simulate rainfall at a volume representative of a typical storm in the region. The intensity varied among fills based on the water pressure available from the pump; in Bearwallow's case, the pressure was likely higher because water was flowing strongly into the pump from a water tank, while at the other fills the pump was drawing water up from an open effluent stream. We performed subsequent ERI surveys after one, two, three, and four hours of sprinkling. At Bearwallow, the effluent stream is intermittent and was dry during much of the field season, so the water source was a tank stationed at the bottom of the fill. At the other three sites, the effluent stream served as the water source for the artificial rainfall. The artificial rainfall setup consisted of a Koshin SERH-50V pump with a Honda GX160H OHV engine, used with a 2-inch diameter, 3.5-meter (11.5-foot) inlet tube and anywhere from 30.5 to 83.8 meters (100 to 275 feet) of 2-inch diameter fire hose carrying water up the slope. The fire hose was then connected to three Orbit oscillating sprinklers via 17 to 18.8 meters of standard garden hoses (Figure A-5 through A-8).

Table 3-3. Summary of Short Artificial Rainfall ERI Surveys

Date	Fill	Transect Length (m)	Electrode Spacing (m)	Length of Fire Hose (m)	Total Length of Garden Hose (all branches, m)	Average Rainfall Intensity (cm/h)	Days since Last Rainfall*	Average SC of Pumped Water* (µS/cm)
08/18/2017	Barton Hollow	50.4	0.8	45.7	17	1.04	2	1519
08/21/2017	Office Fill	63	1.0	30.5	17	1.04	3	2508
08/26/2017	End Fill	63	1.0	83.8	17	1.12	3	2151
09/22/2017	Bearwallow	43.4	1.4	45.7	18.8	2.82	8	988

**Figure D-1, D-2*

3.1.3 ERI Data Analysis

We downloaded the data files from the resistivity meter to a computer and then processed them using EarthImager 2D, a software produced by AGI for use with the SuperSting resistivity system (AGI 2009). The basic inversion process begins with an assumption of homogeneous earth and proceeds to optimize for a model that minimizes the differences between the model and the surveyed apparent resistivity while also maintaining a specified degree of smoothness in the model (AGI 2009). We first adjusted the initial settings in the program to values recommended in the software manual. These initial settings filtered out any raw apparent resistivity data points that were negative, below 1 ohm-meter or above 10000 ohm-meters, as well as any measurements for which the voltage was below 0.2 millivolts. The minimum absolute value of the voltage normalized by the current was 0.0005 ohms. The maximum repeat error acceptable was 3% while the maximum reciprocal error was 5%. These settings are similar to those used by Langston et al. (2011), Johnson et al. (2012), Travelletti et al. (2012), and Greer et al. (2017).

We read the data file of a dry survey into the program and viewed the data editing statistics that EarthImager produced. These statistics detailed how many raw data points, if any, did not meet the criteria specified in the initial settings; the program would automatically remove these prior to the inversion process. Next, we read a terrain file into the program, written using the clinometer data gathered at each fill. The terrain file provides the horizontal location and z-component (elevation) of each change in slope along the transect, and the software calculates the coordinates of each electrode in the survey line.

We ran the inversion using the settings suggested for surface models in the 2009 AGI manual. We used a smooth model inversion method and a finite element forward model method with a Cholesky decomposition and a Dirichlet boundary condition. The model had 2 mesh divisions, and the thickness incremental factor and depth factor were both 1.1 (Greer et al. 2017). The smoothness and damping factors were both 10, default values. We maintained the default estimation that 3% of the data were noisy, and opted to suppress the weights of noisy data during the inversion process to improve the quality of the results and reduce the L2-norm, an error statistic (AGI 2009). Furthermore, we restricted the calculated resistivity values to the default range of 1-10,000 ohm-meters to reduce noise. We set the inversion to stop after any of the following criteria were met: after the eighth iteration, when the root mean square error was below 3%, or when the root mean square error decrease between iterations was below 5% (AGI 2009, Greer et al. 2017). These settings reduced the overall error in our results, as evidenced by

the root mean square error (Equation 3-1) and L2-norm (Equation 3-2) statistics we obtained, and this translated to less noise in the tomograms.

$$RMS = \sqrt{\frac{\sum_{i=1}^{N}\left(\frac{d_i^{pred} - d_i^{meas}}{d_i^{meas}}\right)^2}{N}} \times 100\% \quad (3\text{-}1)$$

$$L2_{Norm} = \frac{\sum_{i=1}^{N}\left(\frac{d_i^{pred} - d_i^{meas}}{W_i}\right)^2}{N} \quad (3\text{-}2)$$

where N is the number of data points; d^{pred} and d^{meas} are respectively the predicted and measured data point, and W is the weight of the data point assigned using a diagonal data weighting matrix determined by assumed data error (LaBrecque et al. 1996, AGI 2009).

Once the initial inversion was complete, we removed any data points with over 50% misfit, defined as the percent error of the calculated data with respect to the measured apparent resistivity (AGI 2009), and reran the inversion. We repeated this process until all of the processed data points were less than 50% misfit, signifying low noise levels within the data. For all but one survey, less than 10% of the data points were removed. For the long transect survey at Bearwallow, 17% of data points were removed. Most of the data points removed in the Bearwallow long-transect survey were linked to one electrode that returned poor data; this was likely a result of a malfunction or poor electrode-earth connection.

For the artificial rainfall surveys, we subsequently conducted the time-lapse inversion, with the later wet surveys compared to the initial dry survey. This yielded a net difference in electrical conductivity (reciprocal of resistivity) between the dry and wet surveys. The program produced four tomograms comparing each of the four wet surveys to the dry survey, showing by what percentage the conductivity of each data point changed.

Once we had produced and scaled all of the tomograms (Appendix E), we cropped them to a reasonable depth of investigation, i.e. a maximum depth of roughly one-fifth of the surface length of the survey (Oldenburg and Li 1999, Greer et al. 2017). This had the result of removing some potentially misleading information at the bottom of each tomogram.

3.1.4 Preferential Infiltration Flowpath Properties Estimation

Using the short artificial rainfall tomograms, we identified accumulation zones, or regions at depth where conductivity increased rapidly, suggesting the presence of preferential infiltration flowpaths from the surface to those points. We estimated each flowpath's length as the depth to the center of the accumulation zone, and the transit time as the time the accumulation zone first appeared on our tomograms relative to the beginning of the artificial rainfall. We then calculated the approximate linear velocity of water within each flowpath using the flowpath length and transit time.

3.2 Verification of ERI results

To verify ERI interpretations, we conducted a series of hydrogeologic investigations at Office Fill and End Fill including fluorescent dye tracing, borehole drilling, and soil infiltration

and excavation. Based on patterns in ERI tomograms (especially evidence of rapid infiltration to depth) and logistical considerations (valley fill size and accessibility to a drilling rig), we initially chose Office Fill for ERI-verification activities. However, after our first attempt at dye tracing at Office Fill in August 2017 failed because of a faulty fluorometer, in consideration of the unknown residence time of the dye previously applied to Office Fill, dye tracing activities were relocated to End Fill in October 2017. Since access for a drilling rig was not available at End Fill, drilling was conducted at Office Fill.

3.2.1 Borehole and Down-hole Video

We hired a well-drilling firm to bore a vertical hole in Office Fill at a point along an ERI transect showing strong contrast in resistivity within 30 m of the surface (see Appendix F for photographs). The intent was to see how accurate our ERI-based interpretations (Section 3.1 above) of subsurface structure and subsurface moisture content distribution were. The moisture content distributions would in turn inform our ERI interpretations of deeper infiltration patterns within the valley fill. The borehole was located on a lift (constructed flat terrace) 143 m up the slope (along the land surface) from the bottom of the valley fill. An HQ-sized drill produced a 96 mm diameter hole and a 63.5 mm diameter core for inspection and possible analysis. After drilling, the sides of the borehole were observed using a down-hole video camera (model GVMICROM1, Marks Products, Inc., Williamsville, VA).

We chose core drilling as the most effective method to drill a vertical borehole through coarse unconsolidated mine spoils, while allowing a video camera to be safely deployed via a cased hole. The camera was lowered to the bottom of the casing then set to record as the casing and camera were slowly raised, such that the casing protected the camera from falling rock. Video was recorded in a series of "takes" starting at the bottom of the borehole. A take included lowering the camera to the bottom of the casing then recording as the casing was raised 3 m (the length of a section of casing). Between takes the camera was removed from the borehole, a section of casing removed from the top end, then the camera was lowered back to the bottom of the casing for the next take.

3.2.2 Artificial Rainfall with Tracer

We applied fluorescent dye tracer (rhodamine WT or RWT) to a valley fill and monitored tracer concentration in the effluent stream. The intent was to monitor the tracer where the effluent stream emerges from the bottom of the valley fill, determine transit times of water over and through the valley fill by various flowpaths, and in combination with flow hydrographs at the same location, learn something about the relative importance and timing of different source waters in the effluent stream.

Our requirements for a tracer included: high solubility in water; minimal sorption to soil, suspended sediment, streambed, plants, etc.; resistant to photo decay when exposed to direct sunlight for 1–2 days; high detectability range with an in-stream fluorometer; easily separable from background fluorescence; low toxicity; affordable. We chose rhodamine WT (RWT) as the most suitable tracer for these requirements. Other tracers were considered too photosensitive (fluorescein, pyranine, photine CU, amino G acid), toxic (rhodamine B), or highly susceptible to adsorption losses (rhodamine B) or background fluorescence (amino G acid, lissamine FF) (Smart and Laidlaw 1977, Trudgill 1987).

On August 21, 2017, we applied liquid tracer to the artificial rainfall sprinkled on the 6 x 30 m plot concurrent with the ERI conducted at the Office Fill (Table 3-3), and monitored the

effluent stream with a fluorometer (Cyclops-7 Rhodamine WT Logger, Precision Measurement Engineering Inc., Vista, CA). However, the Cyclops data logger failed, and given the unknown residence time of tracer in the fill, we did not repeat the tracer experiment on Office Fill. Instead, we moved to End Fill for a second attempt, including a switch to a different brand of rhodamine sensor, as described below. For this reason we do not provide additional details for the Office Fill tracer study, but rather focus below on the End Fill tracer study.

Because we did not know about rhodamine logger failure at Office Fill by the time we did the artificial rainfall with ERI at End Fill on August 26, 2017 (Table 3-3), we redid the artificial rainfall at End Fill on October 20, 2017 in order to apply the tracer. We simulated a 5-cm rainfall by sprinkling approximately 9,200 L (2,550 L/h × 3.6 h) of stream water onto the plot. A total of 575 mL of 20% RWT liquid (Abbey Color; Philadelphia, PA; item 23470; density = 1.165 g/mL), containing 134 g of RWT, was diluted to 5 L in stream water and injected into the water line upstream of the sprinklers, for an average RWT concentration of 12 mg/L in the sprinkled water.

The sprinkling system (Figure 3-3) comprised: 1) a gasoline-powered water pump (model SERH-50V, Koshin Ltd., Schaumburg, IL) to pump water from a pool in the effluent stream up onto the valley fill; 2) a fire hose (84 m long, 5 cm diameter) to convey water from the gasoline-powered pump to the valley fill; 3) a 5 cm (fire hose) to 19 mm (garden hose) reducer constructed from PVC pipe and fittings; 4) a splitter valve to distribute flow via three 6-m garden hoses to; 5) three oscillating lawn sprinklers evenly distributed along the ERI transect; 6) a 12 V DC variable-speed pump (model QBG, Fluid Metering, Inc., Syosset, NY) to inject the RWT solution into the main water line via; 7) a one-way (backflow preventer) valve teed into the reducer (item 3 above). The water pump was run at full throttle, and the RWT pump was set to 40% of maximum flow rate.

Figure 3-3. Water pump (left) and rhodamine WT injection and sprinkling system (right) used in artificial rainfall with tracer experiments in August and October 2017.

We deployed a fluorometer (model 6920 sonde with 6130 RWT sensor and 6136 turbidity sensor, YSI Inc., Yellow Springs, OH) in the effluent stream before the RWT application. The sonde logged temperature-compensated RWT concentration (µg/L) and turbidity (NTU) at 10 minute intervals. The fluorometer was calibrated (2-point) in stream water (blank) and RWT diluted to 20 µg/L in stream water. The mass (g) of RWT discharged in the effluent stream was calculated as the sum of the products of RWT concentration and stream flow across all 10-min intervals (after linearly interpolating stream flow from 15- to 10-min intervals). RWT concentrations less than the method detection limit (MDL; estimated as 3 × SD of baseline in-stream RWT readings recorded during the first two days of RWT logging (USEPA 2016) were excluded from the sum. The RWT mass balance was calculated with and without accounting for turbidity interference (assuming 0.03 µg/L of apparent RWT per NTU per YSI (2012)).

3.2.3 Soil Pits and Infiltration

We excavated soil pits along the Office Fill and End Fill ERI transects in areas where a series of ERI tomograms taken during artificial rainfall showed apparent flowpaths (see Appendix G for photographs). The intent was to see if we found evidence for our ERI interpretations (Section 3.1 above) of preferential flow through the surface layer (top ~ 1 m). At Office Fill on August 22, 2017, soil pits were excavated to a depth of 75–110 cm by mini-excavator at two stations along the ERI transect: Station 1 located on a lift 32–39 m from the bottom of the valley fill, where ERI showed a moderate increase in conductivity centered at 2.4 m below the surface; Station 2 located on a steep hillslope 23 m from the bottom of the valley fill, where ERI showed a strong increase in conductivity centered at a depth of 2 m.

At End Fill on October 25, 2017, we sprinkled 20 L of blue dye solution (Standard Blue Powder, Kingscote Chemicals, Miamisburg, OH diluted to 6 g/L in stream water) on each of four 0.5 × 1 m plots located along the ERI transect. The long axis of each plot was oriented parallel to the hillslope. The dye was sprinkled on a plot for 5–10 minutes using a plastic tub with 1.6 mm holes drilled on a 2.5 cm grid in the bottom, supported by a leveled wooden frame (Clark and Zipper 2016). Two hours after the dye was applied the plots were hand dug to a depth of 0.5 m. A vertical face was exposed starting at the downhill end of the plot. Digging continued upslope to the upper end of the plot, with pauses to describe and photograph dye flowpaths encountered.

3.3 Monitoring Streams and Natural Rainfall Events

3.3.1 Effluent Stream Monitoring

We monitored the effluent stream draining each of the four valley fills (Figure 3-1) to analyze basic statistics of channel discharge (Q), water balance, and electrical conductivity (EC) variation among effluent streams; and analyze relationships between Q and EC as these relationships can provide insight into solute sources within a watershed. Discharge and EC records are also useful general background information for the larger study.

During May–December, 2017, we continuously monitored (15 minute increments) EC, temperature, and Q of the four valley fill effluent streams, along with local rainfall at each valley fill. Rainfall was monitored with a Rain Collector II 2 mm tipping-bucket gauge by Davis Instruments in conjunction with a HOBO UA-003-64 event logger by Onset. EC and water temperature were logged (model HOBO U24-001, Onset Computer Corporation, Bourne, MA) then converted to specific conductance (SC) at 25 °C using the non-linear method for natural waters (International Organization for Standardization, ISO, 1985:7888). EC sensors were cleaned monthly, and each monthly data series was adjusted for sensor drift (assuming linear drift) using starting and ending calibration readings taken with a portable meter.

We monitored discharge at End Fill, Barton Hollow, and Bearwallow using trapezoidal flumes (Trapezoidal Flume No. 1, as described by (Robinson and Chamberlain 1960) and built in Richard Warner's Lab, University of Kentucky, Lexington), and at Office Fill using a 3-inch Parshall flume (Engineered Fiberglass Composites Inc., New Lisbon, WI). Each flume was equipped with a pressure (water-level) logger (model HOBO U20-001-01, Onset Computer Corporation, Bourne, MA) mounted in a stilling well. To correct for changes in atmospheric pressure we used a separate pressure logger mounted in air at a central location within 2 km of each flume. Flumes were cleaned and water-level loggers calibrated monthly.

The relationship between water level (stage) and Q for Trapezoidal Flume No. 1 (Robinson and Chamberlain 1960) is:

$$Q = 0.01780\,H^{2.5} + 0.106\,H^{1.5} + 1.42 \quad (3\text{-}3)$$

where Q = discharge (L/s); H = stage (cm) at the entrance to the flume's converging section. Equation 3-3 was validated over a flow range of 4.5–201 L/s, equivalent to H = 6–39 cm. Since stage was frequently <6 cm in our flumes, we developed the following flume-specific low-flow H–Q rating curves by regressing reference Q measurements (13 at End Fill, 6 at Barton Hollow) against water level:

$$Q_{\mathrm{EF}} = 2.2946H + 0.5622 \quad (3\text{-}4)$$

$$Q_{\mathrm{BH}} = 0.187H^{1.7133} \quad (3\text{-}5)$$

where Q_{EF} = discharge (L/s) at the End Fill flume, and Q_{BH} = discharge at the Barton Hollow flume. The observations used to develop Equations 3-4 and 3-5 had H ranges of 0.3–4 cm (End Fill) and 3.3–6.7 cm (Barton Hollow).

We used Equation 3-3 when $H \geq 6$ cm, and Equations 3-4 and 3-5 when H <6 cm. We measured the reference discharge observations directly using the median time (of three trials) to fill a 19 L bucket. At End Fill the bucket was filled at the outlet of a perched road culvert located <20 m downstream of the flume. At Barton Hollow the flume outlet was temporarily fitted with a plywood dam with a 10 cm diameter × 3 m long overflow pipe spilling into the bucket. Because of low gradient and large boulders near the outlet of the Bearwallow dam, no reference discharge measurements were taken at Bearwallow. Since the Bearwallow and Barton Hollow flumes were both installed nearly level longitudinally, whereas the End Fill flume sloped, the Barton Hollow low-flow rating curve was used at Bearwallow.

The H–Q relationship for the 3-inch Parshall flume at Office Fill is:

$$Q_{OF} = 0.1422H^{1.547} \quad (3\text{-}6)$$

99.9% of the stage readings from Office Fill fell within the range for which Equation 3-6 was validated (3–35 cm) (Teledyne Isco 2013), so no alternate H–Q equation was needed.

We calculated water balance for each valley fill by month. First, monthly unit-Q (Q_{U}, m^3/ha) was calculated as the total volume of water discharged in a month (m^3) divided by the total watershed area upstream of a flume (A_{T} = 25.3 ha, 30.4 ha, 41.5 ha, and 53.3 ha, respectively, for Bearwallow, End Fill, Office Fill, and Barton Hollow). Then Q_{U} was expressed as % of monthly rainfall per ha (Q_{R}). To estimate the fraction of stream flow originating from the valley fill footprint (Q_{VF}), we multiplied Q_{R} by valley fill footprint area (A_{VF} = 15 ha, 1.5 ha, 2.8 ha, and 7.0 ha, respectively) and divided by A_{T}. The watershed contributing to each flume was delineated from the National Elevation Dataset (10 m resolution) (USGS 2013) using hydrology tools in ArcGIS 10 s, (ESRI, Redland CA). We measured A_{VF} using imagery and the polygon tool available in Google Earth Pro (version 7.1.8.3036, Google Inc., Mountain View, CA). For an alternate view of the contribution of rainfall on a valley fill to effluent stream discharge, we also calculated the ratio (percent) of rainfall on a valley fill (estimated by multiplying recorded rainfall by A_{VF}) to monthly effluent stream discharge.

To examine relationships between SC and *Q*, which are influenced by hydrologic flowpaths and source-water ionic concentrations, we plotted SC versus *Q* for individual rain events and analyzed hysteresis patterns.

3.3.2 Natural Rainfall with Tracer

For a particular storm event, we dispensed concentrated RWT across an entire valley fill the day before predicted rainfall, followed by in-stream monitoring of RWT concentration for reasons similar to those during artificial rainfall (see Section 3.2.2 above). On December 4, 2017, after deploying a fluorometer (as described above) in the effluent stream, we applied 28.0 kg (24.1 L) of 20% RWT liquid (equivalent to 5.61 kg of RWT) across approximately 85% of a 1.5 hectare valley fill (End Fill). We did not apply RWT to the lower 15% of the valley fill in order to avoid spraying RWT into seeps where the effluent stream emerged near the toe of the valley fill. A similar amount of 20% RWT was applied per m^2 in the natural and artificial rainfall experiments (2 and 3 mL/m^2 respectively). Starting at a top corner of the valley fill, the four crew members lined up 2 m apart (up and down the hill) and traversed back and forth across and down the valley fill while dispensing RWT from handheld sprayers. To ensure the RWT supply was not exhausted before reaching the bottom of the valley fill, spraying was intermittent, with crew members instructed to spray during three of every six steps. RWT mass balance was calculated as described above.

3.4 Relating Valley Fill Geology with Effluent Hydrology and Water Quality

We performed simple linear regressions on a variety of quantitative fill and flowpath properties. Independent variables were age of the fill since reclamation, fill area, and drainage basin area (Table 3-1). We analyzed these in relation to the potential dependent variables of preferential infiltration flowpath length, transit time, and velocity. Finally, we analyzed SC of the fills' effluent streams as a possible variable dependent on any of the named fill or flowpath properties.

4. RESULTS AND DISCUSSION

4.1 Electrical Resistivity Imaging (ERI) of Valley Fills

4.1.1 Results

4.1.1.1 Long dry ERI surveys

Figure 4-1 shows tomograms, which are vertical cross sections of estimated electrical resistivity distribution beneath the transects shown by white dashed lines in Figure 3-1 and summarized in Table 3-2. In general, we associate low resistivity values with fine materials and soil-sized particles that retain water well, as the water will conduct an electrical current and thus lead to a low electrical resistivity. Meanwhile, high resistivity values may represent boulders, bedrock, or large void spaces (Greer et al. 2017).

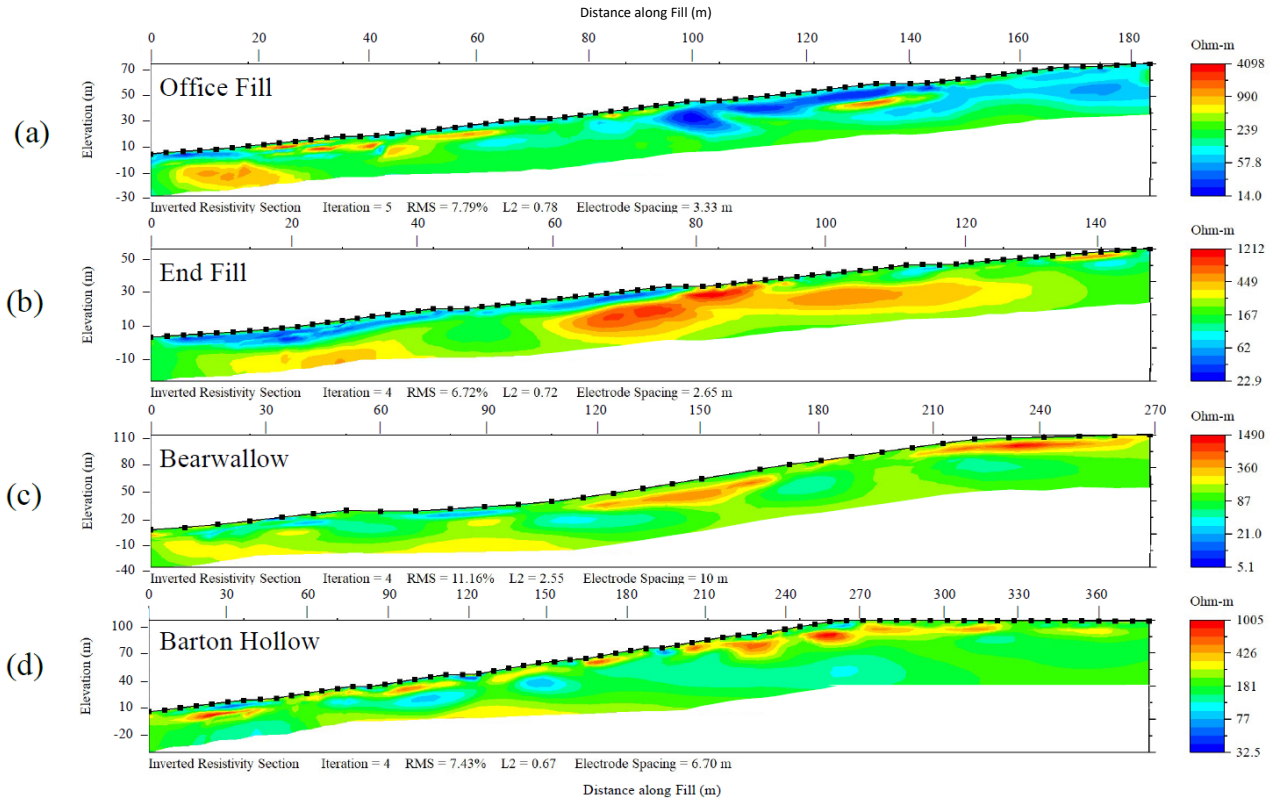

Figure 4-1. Long dry survey ERI tomograms depicting transects of the four sites: (a) Office Fill; (b) End Fill; (c) Bearwallow; (d) Barton Hollow. Each tomogram uses the default resistivity color scale generated by EarthImager 2D based on the range of resistivities calculated for that section. Elevation values are relative to the base of the transect at the toe of the fill. Note differences in spatial and resistivity scales among fills.

There are interesting features of the tomograms for each individual fill. At Office Fill (Figure 4-1a), the upper half of the slope shows a large section of low resistivity at shallow depth. This suggests a thick layer of soil-sized particles that retains water near the surface in the absence of large pore spaces, which are often associated with larger voids between boulders or other coarse material. Office Fill experienced natural rainfall within a week prior to the survey (Table 3-2), and this likely contributed to the wide low-resistivity layer.

At End Fill (Figure 4-1b), a low resistivity layer exists at very shallow depths over the lower half of the fill. Because End Fill is >20 years old, there has been time for development of forest vegetation and soil with moisture retention capacity at the fill surface; and it appears that the rain that fell just two days prior to the survey may have stayed near the surface. By contrast, the low-resistivity area near the top of End Fill is less extensive, occurs at greater depths, and is overlain by a high-resistivity area. This would be consistent with layers leached of conductive salts over time as described by Greer et al. (2017) or with a thin layer of soil-sized particles and more boulders nearer to the surface. There is also a very large area of high resistivity at greater depths, observed around 60-80 horizontal meters. The combination of low resistivity at shallow depths and greater resistivity at greater depths is expected from conventional fill construction, which consists of dumping boulders down the slope and then covering them with finer material. This pattern is consistent with that described by Greer et al. (2017).

Neither Bearwallow (Figure 4-1c) nor Barton Hollow (Figure 4-1d) shows the same large sections of homogeneous resistivity as Office Fill and End Fill, indicating more structural heterogeneity in the subsurface. The absence of large regions of low resistivity may also be due to the longer elapsed time between a natural rain event and the surveys (Table 3-2), associated with less antecedent moisture in the ground. Additionally, the different-colored resistivity sections in the Bearwallow tomogram do appear more elongated than those in Barton Hollow. This may be due to the increased electrode spacing at Bearwallow which required the software to interpolating data points over a longer lateral distance.

At Bearwallow, the top of the transect was non-fill material, i.e., unmined land. This transition from fill to unmined occurred between the 26^{th} and 27^{th} electrodes from the bottom, or around 224 horizontal meters. The tomogram shows a solid slab of high resistivity near the surface of this unmined section; given our knowledge about the undisturbed section of land, this slab may signify unbroken bedrock or leached material as described above. This high-resistivity region transitions downslope to an area with more moderate resistivity and ends around 215 horizontal meters. There is no clear break in the tomogram where the shift from fill material to non-fill material occurs, likely because the software is cross-referencing data from multiple electrodes to create this image, thereby smoothing any sharp gradients that might otherwise appear. Another high-resistivity area appears around 150 horizontal meters, but we know this area contains deep fill material and therefore the slab cannot realistically be undisturbed bedrock. In this case, it may represent large boulders with large voids that do retain much fine-grained materials and therefore retain little moisture.

At Barton Hollow, low and high resistivity sections are interspersed throughout the fill, and none of these regions are laterally or vertically extensive. High resistivity regions often appear above low resistivity, suggesting the presence of high-resistivity boulders with sizable intervening void spaces that allow water to migrate deeper past the boulders.

There are also a number of interesting patterns that emerge when considering all of the fills together. Figure 4-2 assists this comparison process by showing tomograms where the resistivity color bars have uniformly set to the same resistivity scale.

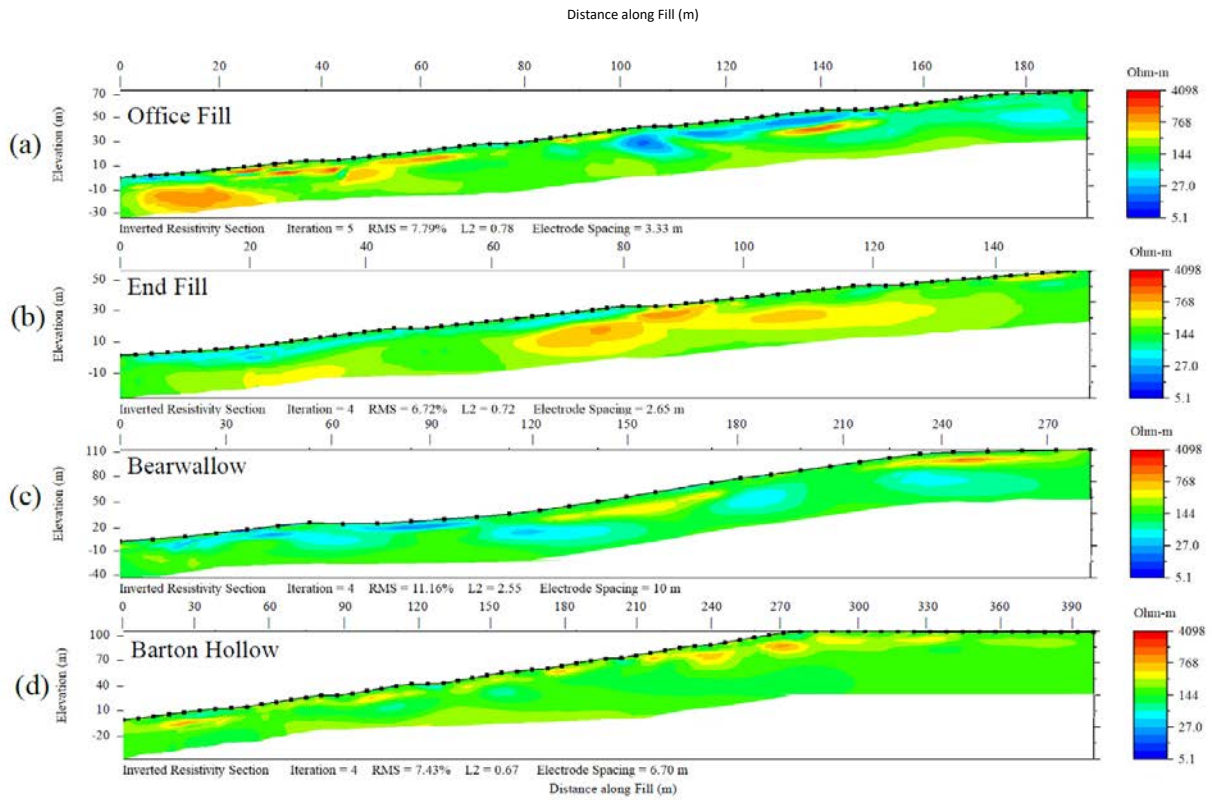

Figure 4-2. Long dry survey ERI tomograms depicting transects of the four sites: (a) Office Fill; (b) End Fill; (c) Bearwallow; (d) Barton Hollow. Each tomogram has the same resistivity color scale to facilitate comparisons among fills. Elevation values are relative to the base of the transect at the toe of the fill. Note differences in spatial scale among fills.

Office Fill shows by far the largest range in resistivity of the four fills, followed by Bearwallow. Barton Hollow and End Fill, by contrast, showed less variation in resistivity (Figure 4-2). The tomograms of Barton Hollow and Bearwallow show the most heterogeneity on a small scale. In other words, they show many small regions of differing resistivities compared to End Fill and the top of Office Fill, which show fewer large regions of differing resistivities. It is worth noting that Office Fill's and End Fill's small sizes (as represented by the horizontal scale) make their areas of differing resistivities appear larger, relative to Barton Hollow and Bearwallow. Still, End Fill and particularly Office Fill display large resistivity regions, even when the tomogram scales are taken into account.

4.1.1.2 Short artificial rainfall ERI surveys

Figure 4-3 through Figure 4-6 show time-lapse tomograms from the short surveys with artificial rainfall. Unlike the long transect tomograms in Section 4.1.1.1 above, which simply depict a snapshot of the resistivity within the fill's subsurface, these images compare the fill at the time of the survey to a dry baseline state. As such, EarthImager can represent this comparison as percent difference of either resistivity or conductivity, and the latter is recommended for decreasing-resistivity scenarios such as the water infiltration we implemented (AGI 2009). Increasing conductivity indicates increasing moisture due to water's ability to conduct an electrical current. Note that any apparent decreases in electrical conductivity are artifacts of the inversion process that appear in response to a contrast boundary, in this case a nearby increase in conductivity (AGI, 2009; Nimmer et al., 2008). They cannot be realistically interpreted as

sections of the ground becoming drier during the four-hour rainfall period (Miller et al. 2008, Pellicer et al. 2012, Mojica et al. 2013, Greer et al. 2017).

The time-lapse tomograms are helpful for identifying preferential flowpaths of infiltrating rainwater. We distinguish two main types of preferential infiltration flow in terms of how they manifest in the tomograms. Type I results in wetted regions at depth, referred to as accumulation zones by Greer et al. (2017), without a pathway visible in successive ERI surveys. This suggests rapid and mainly vertical water movement along a flowpath where the flowpath itself does not retain a noticeable amount of water after the fact. It is also possible that the flowpath retains a significant amount of water but that its shape or positioning makes it difficult for an ERI survey to image. In Type II preferential infiltration flow, the flowpath itself appears on the tomogram but does not result in an isolated accumulation zone; these flowpaths tend to be more diagonal or horizontal. Type I flowpaths appear in our tomograms far more frequently than Type II.

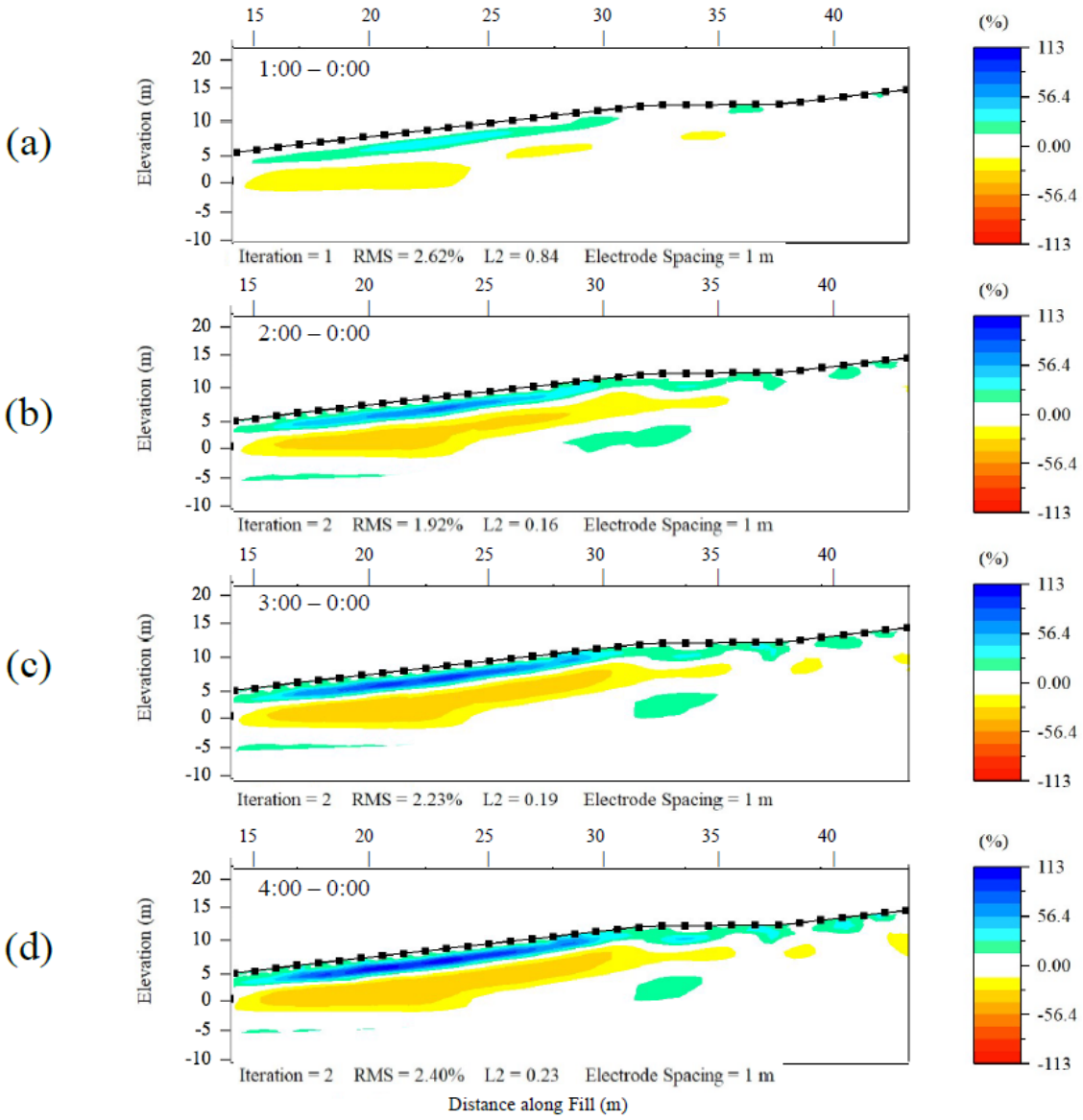

Figure 4-3. Short ERI tomograms of the artificial rainfall plot at Office Fill, cropped to show only the wetting zone. Each tomogram shows the percent difference in electrical conductivity, relative to a dry baseline survey, after (a) one; (b) two; (c) three; and (d) four hours of sprinkling. Elevation and horizontal distance values are relative to the toe of the fill.

At Office Fill, the rainfall plot covered most of the fill's bottommost lift and a small part of the second lift. The tomograms reveal a consistent layer of increasing conductivity (Figure 4-3). This overlays a thicker layer that does not increase in conductivity during the rainfall period. The is consistent with structural interpretations from the long surveys, including a top layer that is likely primarily finer materials that retain water well overlaying larger rocks and boulders which do not. There is an accumulation zone at approximately 33 horizontal meters and 10.5 meters of depth from the surface. It first appears in Figure 4-3b after two hours of sprinkling and is roughly beneath a point near the surface that also becomes noticeably wetter over time.

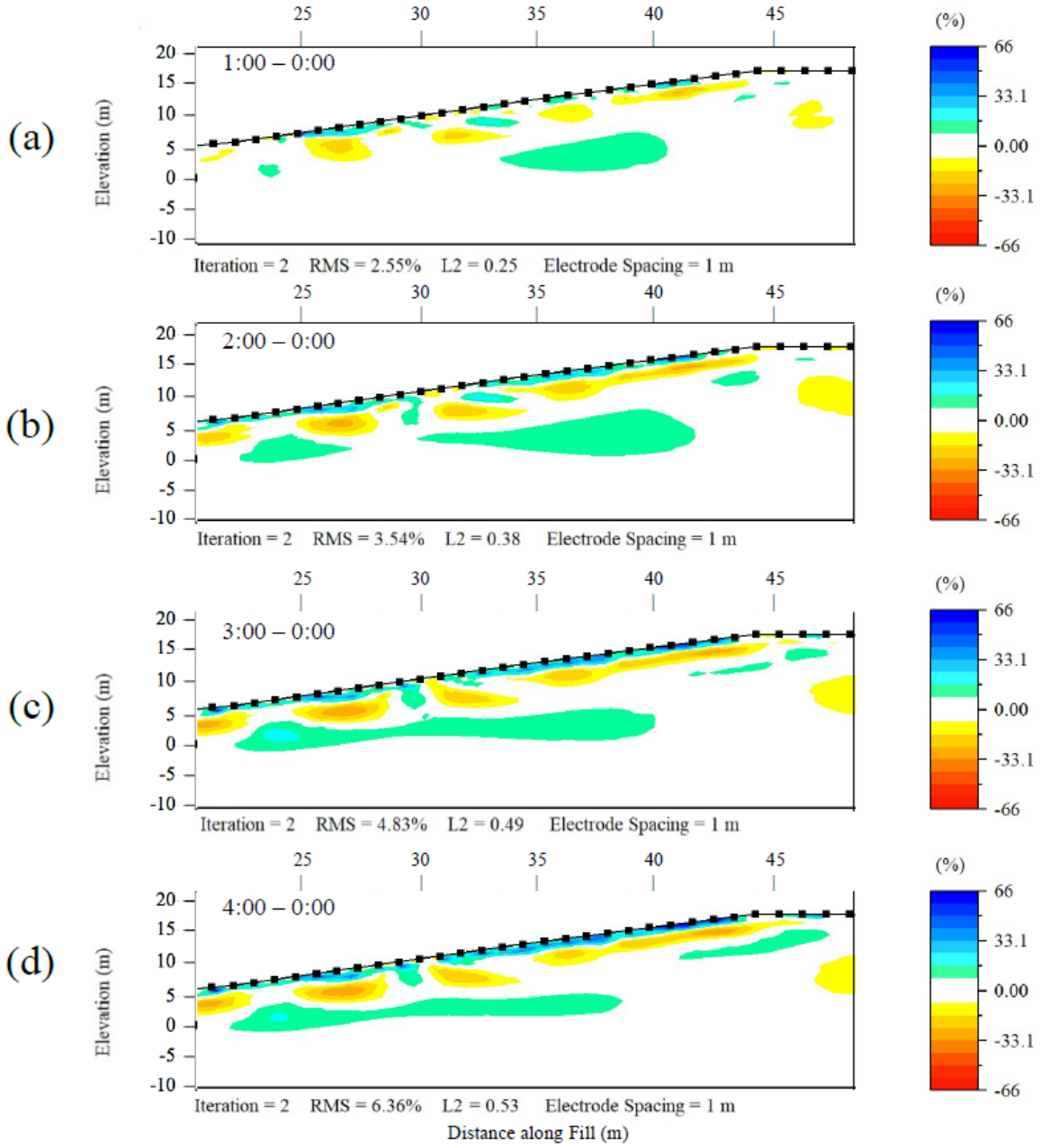

Figure 4-4 Short ERI tomograms of the artificial rainfall plot at End Fill, cropped to show only the wetting zone. Each tomogram shows the percent difference in electrical conductivity, relative to a dry baseline survey, after (a) one; (b) two; (c) three; and (d) four hours of sprinkling. Elevation and horizontal distance values are relative to the toe of the fill.

At End Fill, the water applied via artificial rainfall fell on the top half of the bottommost lift. It then made its way to many different locations in the fill, indicated by blue increasing-conductivity areas that appear in later tomograms (Figure 4-4). Some of these increasing moisture areas occur in shallow layers, perched atop regions that do not increase in conductivity, for example near 20, 25-27, 32-37, and 40-43 horizontal meters. This indicates that the surface became wetter and retained water, but this zone is much thinner than those observed at Office

Fill and Barton Hollow. This pattern of very shallow retention is consistent with the development of a soil-like layer at the surface, to a depth of approximately 0.5 to 1 meter, through the action of plants and root development. One other notable pattern that may be a visible flowpath to depth, representing Type II preferential infiltration flow, occurs just below the surface at approximately 30 horizontal meters and develops in size and degree of saturation over time.

Multiple deeper accumulation zones also occur at End Fill. A few of these areas appear after one hour of sprinkling, at 23.5 horizontal meters and 5.5 meters of depth and at 37 horizontal meters and 10.5 meters of depth. Because the tomograms show no visible vertical flowpaths (i.e. areas of increasing conductivity) connecting these areas to the surface, these deeper accumulation zones represent Type I preferential infiltration flow. The water appears to have rapidly infiltrated down heterogeneous pathways, i.e., pathways through layers of various resistivities and particle sizes (Figure 4-4). The saturated region at depth also appears to spread out and migrate downslope into a consistent horizontal region underground, from about 22 to 40 horizontal meters, over the course of the water application. It is unclear whether this is due to horizontal motion of water already at depth or to additional vertical flowpaths developing that did not contribute to the moisture at depth after one hour. In either case, the manner in which this accumulation zone flattens out deep in the fill suggests that it may have reached the bottom of the dumped fill material, which would be underlain by undisturbed materials.

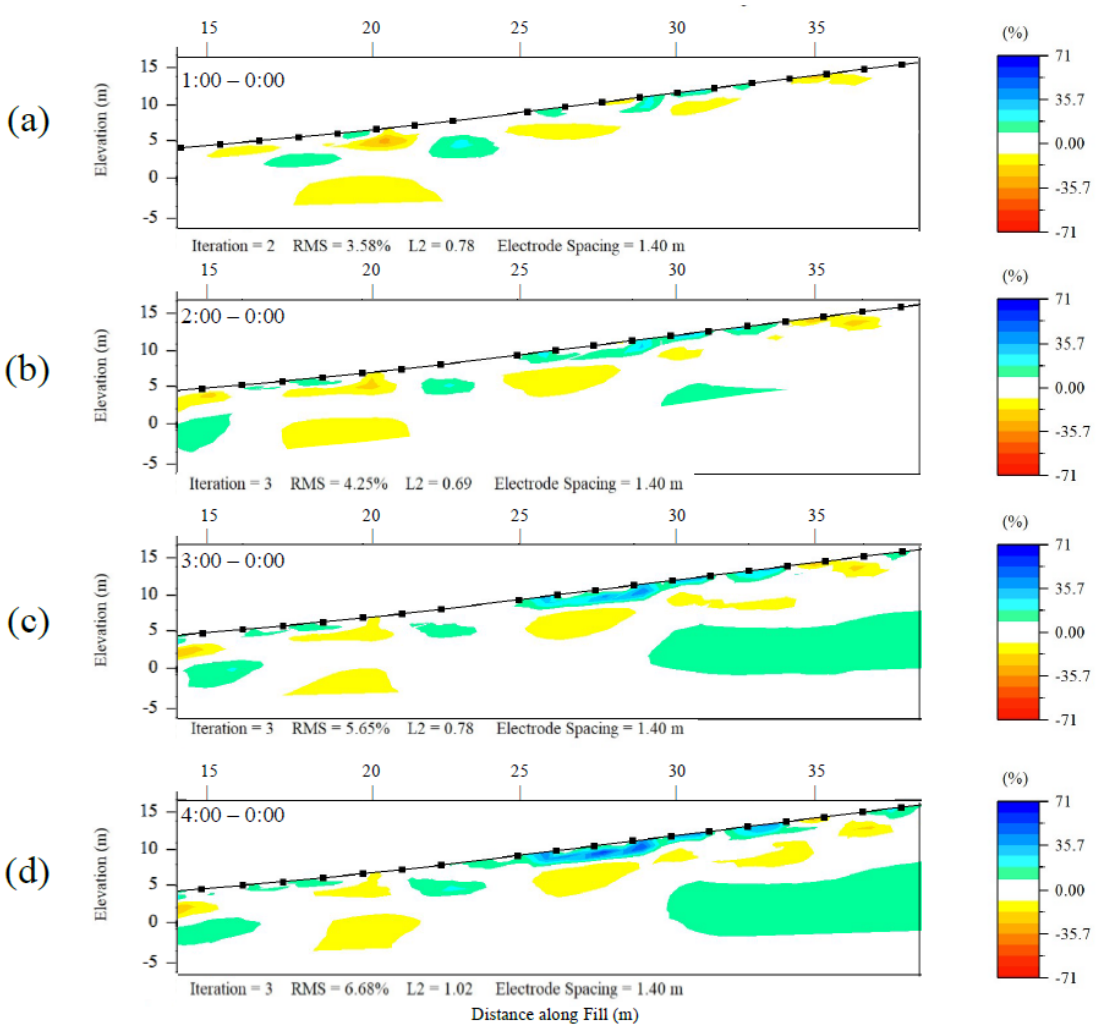

Figure 4-5. Short ERI tomograms of the artificial rainfall plot at Bearwallow, cropped to show only the wetting zone. Each tomogram shows the percent difference in electrical conductivity, relative to a dry baseline survey, after (a) one; (b) two; (c) three; and (d) four hours of sprinkling. Elevation and horizontal distance values are relative to the toe of the fill.

The artificial rainfall plot at Bearwallow was near the bottom of the fill. At Bearwallow, there are fewer areas of increasing electrical conductivity at shallow depth relative to other fills (Figure 4-5). The only large area of moisture accumulation is from 25-29 horizontal meters, while a smaller moisture-accumulation area occurs at 29-34 horizontal meters. These shallow areas saturate slowly and grow in size late in the four-hour sprinkling period (Figure 4-5cd). These overlie areas that appeared to decrease in conductivity, which are artifacts of the data inversion rather than physical phenomena. Still, these areas' apparent decrease in conductivity suggests that they did not become and remain significantly wetter during the rainfall period. One possible explanation for these areas is the presence of boulders or other materials with voids and/or large pores that do not retain moisture.

There are a few visible accumulation zones due to Type I preferential flow. For example, such regions appear at 3.5 meters below the surface at 23 horizontal meters, and also at 3.0 meters deep at 17.5 horizontal meters, after one hour of sprinkling (Figure 4-5a). The latter disappears in subsequent tomograms, suggesting that the water continued to move away so that

the region was no longer significantly wetter than its base case state. After two hours, an accumulation zone appears at 5.0 meters deep at approximately 15.5 horizontal meters, and another at 32 horizontal meters and 9.0 meters deep (Figure 4-5b). Water may have collected in these deeper areas due to the presence of fine particles that retain moisture. The accumulation could also be due to an impermeable layer below them preventing further downward flow; we do not know how deep below the fill surface the undisturbed bedrock lies.

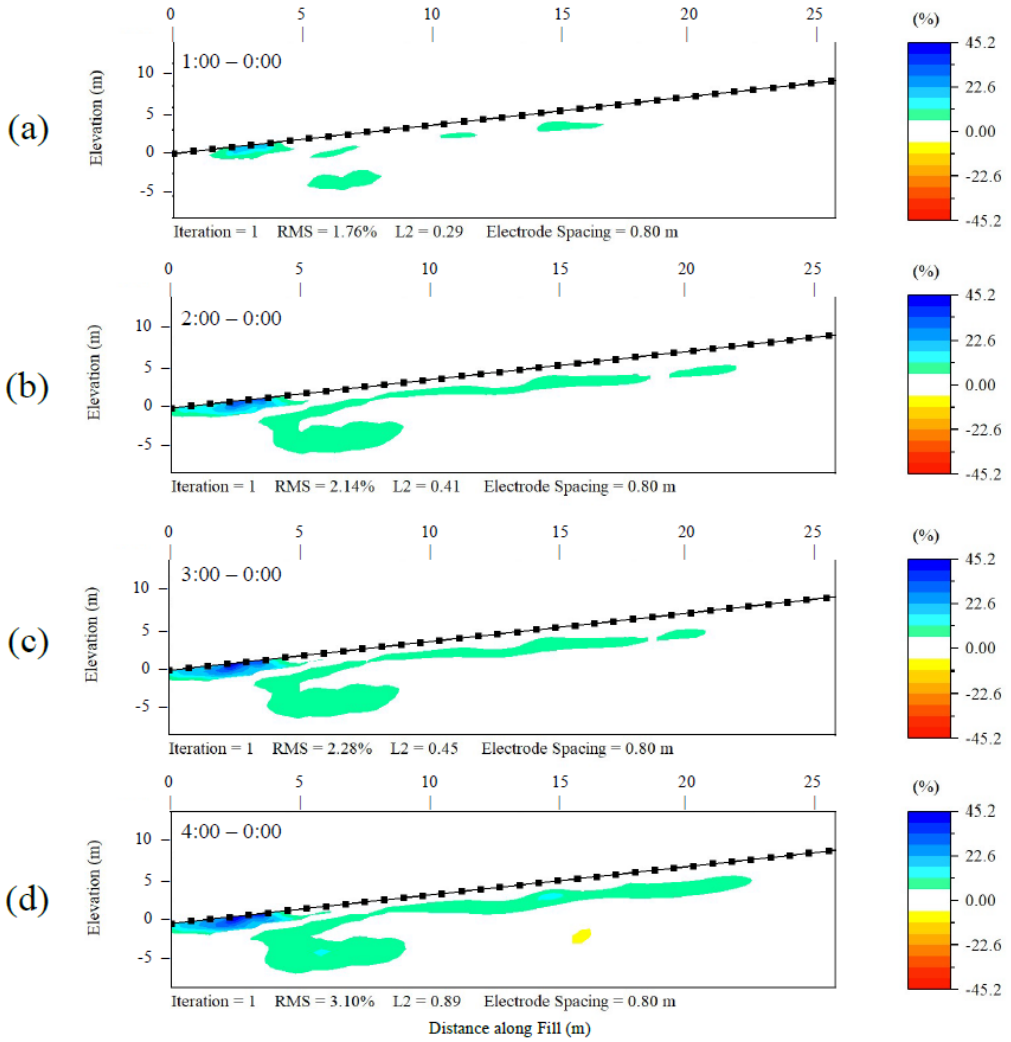

Figure 4-6. Short ERI tomograms of the artificial rainfall plot at Barton Hollow, cropped to show only the wetting zone. Each tomogram shows the percent difference in electrical conductivity, relative to a dry baseline survey, after (a) one; (b) two; (c) three; and (d) four hours of sprinkling. Elevation and horizontal distance values are relative to the toe of the fill.

The wetting zone at Barton Hollow spanned from the bottom of the fill to about two-thirds of the way up the bottommost lift. At Barton Hollow, a roughly one-meter layer at the surface, from the toe of the fill up to about four horizontal meters, retains moisture (Figure 4-6). One possible explanation for this is the grassy land cover of the fill, similar to that of the valley fill site discussed in Greer et al. (2017). Long grasses have fibrous roots that help to stabilize fine particles and produce organic materials. These resulting soils and organic materials may in turn

keep the water near the surface and prevent most of it from infiltrating to depth quickly. Indeed, Clark and Zipper (2016) found that hydraulic conductivities and infiltration rates were lower at reclaimed surface coal mines with grassy or herbaceous vegetation than at those with woody vegetation. The intentional compacting of a near-surface layer of the Barton Hollow fill, may also contribute to this water retention. It is quite possible that the moisture retained near the surface, both in high amounts near the toe and in lesser quantities along nearly the entire length of the rainfall plot, confirms the presence of this compacted layer and its success in keeping much of the infiltrating rainfall in the shallowest zones rather than allowing it to percolate deeper into the fill material. The upslope regions of the rainfall plot that experienced minimal or no change in resistivity near the surface may result from some of the rainfall running downslope over the surface prior to infiltrating, or from a lower rainfall rate due to lower water pressure near the top of the plot.

However, despite the potential presence of this shallow moisture barrier, we also see a noticeable accumulation zone at approximately 7.0 horizontal meters and 6.0 meters of depth from the surface. It appears in Figure 4-6a after only one hour of sprinkling, and it grows in size and degree of saturation over the course of the experiment. This is likely the product of a primarily vertical preferential infiltration flowpath, perhaps indicating that the compaction was inadequate to fully prevent water from penetrating the fill's interior at this location.

4.1.1.3 Preferential infiltration flowpaths

Type I preferential flow that results in accumulation zones at depth without visible flowpaths in the tomograms can be used to form rough estimates of velocity and transit time within the presumed near-vertical flowpath. Here we summarize notable accumulation zones at depth in Table 4-1. There may have been smaller accumulations present during the experiment, but ERI only images accumulations larger than the ERI's spatial resolution and therefore any flowpaths that resulted in smaller accumulations are invisible in the tomograms. Additionally, some of the subsurface moisture increases captured in the tomograms may have been antecedent moisture moving from prior positions, particularly at Office Fill, End Fill, and Barton Hollow. Bearwallow experienced less precipitation over the course of the field season than the other three sites and the longest intervening time between its last natural rainfall event and the artificial rainfall experiment; therefore it likely had the least moisture initially present.

The time to first appearance of each accumulation zone listed is approximate, since surveys were taken only once per hour. Thus, our reported transit times are overestimates, being greater than or equal to the actual times. The development of the first accumulation zones could have occurred in well under an hour, making the upper end of the uncertainty ranges for transit time potentially quite high. This is likely the largest contributor to uncertainty in transit times. We then approximated the depth of each accumulation zone by visually estimating its center point on the tomogram, measuring the vertical distance to the surface, and performing calculations using the tomogram's vertical scale. Because flowpaths may be non-vertical, and also due to tortuosity of flow around rocks, our reported flowpath lengths are underestimates, being less than or equal to the actual lengths. The uncertainty in both the time and depth measurements in turn both affect the linear water velocity, calculated by dividing the two measured values. Therefore, the water velocity values are useful for observing general patterns but not for calculations requiring precision. Nevertheless, given that the numerator (flowpath length) is an underestimate and the denominator (transit time) is an overestimate we can say that

the velocities are underestimates, with the true values likely being higher. The velocities are loosely correlated to the

Calculated transit times range from 1 to 2 hours, with an average of 1.4 hours and a mode of only 1 hour. Calculated vertical depth range from 3.0 to 10.5 meters, with an average of 6.6 meters. Velocities range from 2.5 to 10.5 m/h with an average of 5.1 m/h, which is 0.14 cm/s, and the actual values are almost certainly higher. These data support the presence of a large number of relatively fast infiltration flowpaths.

Table 4-1: Preferential Infiltration Flowpath Properties

Fill (Figure)	Horizontal Location (m)	Time to First Appearance, or Flowpath Transit Time (h)	Approximate Vertical Depth from Surface, or Flowpath Length (m)	Approximate Linear Water Velocity along Flowpath (m/h)
Office Fill (Figure 4-3)	33.0	2	10.5	5.25-10.5
End Fill (Figure 4-4)	23.5	1	5.5	>5.5
End Fill (Figure 4-4)	37.0	1	10.5	>10.5
Bearwallow (Figure 4-5)	23.0	1	3.5	>3.5
Bearwallow (Figure 4-5)	17.5	1	3.0	>3.0
Bearwallow (Figure 4-5)	15.5	2	5.0	2.5-5.0
Bearwallow (Figure 4-5)	32.0	2	9.0	4.5-9.0
Barton Hollow (Figure 4-6)	7.0	1	6.0	>6.0

4.1.1.4 ERI error analysis

As with any field measurements, variability and associated potential for error occur with ERI. There was variability in the contact and placement of electrodes; we sometimes needed to place them up to a meter away from the center line laterally, or up to about 25 centimeters up and down the transect due to rocks or vegetation. The transect itself had a small degree of sinuosity rather than being completely straight. The surveys' temperature and antecedent moisture conditions also varied throughout the field season; all surveys followed at least 48 hours with no precipitation, but in some cases there had been rain a few days prior and in others the weather had been dry for weeks. Finally, during the data collection we obtained occasional error messages on the resistivity meter, which corresponded to either uncollected or unusable data points later in the process. These errors are all within normal ranges for studies of this kind and through proper filtering and interpretation do not undermine the conclusions we present from this study.

The error incurred in the field was addressed during the data processing, as we removed data points both prior to and after inversion. The raw apparent resistivity data points that did not meet the criteria specified in EarthImager's initial settings were not incorporated into the inversion. After inversion, EarthImager's data misfit histogram feature provides a quantitative display of which inverted resistivity data points do not make sense considering the rest of the picture and allows for their removal. We used this feature and repeated the inversion as many times as necessary to eliminate all points that exhibited over 50% data misfit (Table 4-2). The resulting tomogram still included a bit of error, which was reported as the root mean square (RMS) error and the normalized L2 value (Table 4-3).

Table 4-2. Data Removal in Long Dry ERI Survey Inversions

Fill	Survey	Raw Data (# Points)	Initial Data Removal (# Points)	Data Removal During Inversion (# Points)	Data Points Remaining (%)
Barton Hollow	Long	895	55	4	93.4%
	Short dry	942	0	1	99.9%
Office Fill	Long	942	26	8	96.4%
	Short dry	942	0	2	99.8%
End Fill	Long	942	0	0	100%
	Short dry	942	0	4	99.6%
Bearwallow	Long	274	29	18	82.3%
	Short dry	273	9	14	91.6%

Table 4-3. Error in Inversion Results

Fill	Survey(s)	Number of Iterations	RMS Error (%)	L2-norm
Barton Hollow	Long	4	7.43	0.67
	Short dry	4	6.15	0.50
	Short wet	1	1.76-3.10	0.29-0.89
Office Fill	Long	5	7.79	0.78
	Short dry	4	5.57	0.68
	Short wet	1-2	1.92-2.62	0.16-0.84
End Fill	Long	4	6.72	0.72
	Short dry	3	8.01	0.97
	Short wet	2	2.55-6.36	0.25-0.53
Bearwallow	Long	4	11.16	2.55
	Short dry	4	8.56	0.82
	Short wet	2-3	3.58-6.68	0.69-1.02

4.1.2. Discussion

4.1.2.1 Surface coal mine valley fill internal structure and hydrology

Our four field sites taken together show significant variation in subsurface structure and preferential hydrologic flowpaths. Most notably, the experimental thin-lift with compaction construction method implemented at Barton Hollow seems to have affected both subsurface structure and preferential infiltration flow patterns during our four-hour experimental storm. The range of subsurface resistivities and the number of deep accumulation zones beneath the artificial rainfall plot were both reduced relative to otherwise similar conventional (i.e. loose-dump) fills. The relatively small resistivity range suggests more consistent structural distribution throughout the fill and may be the result of the intentional construction method used (Figure 3-2), in which most or all of the fill material was likely to produce low levels of TDS (Zipper et al. 2015). This is consistent with the effluent stream SC values, which are the lowest of the four fills (Figure D-1). There are many possible causes, including the placement of high TDS generating rocks away

from infiltrating rainwater, but another may be the physical structure of the fill allowing less water to infiltrate deep into the fill relative to other fills.

The average minimum preferential flow velocity we calculated was 5.1 m/h, or 0.14 cm/s (Table 4-1). Prior studies have shown similar values for subsurface preferential flow. For instance, estimates of mine spoil flows at a mine in eastern Kentucky ranged from ~10-15 m/h (Wunsch et al. 1999). This is similar to other disturbed lands and karst. Travelletti et al. (2012), using ERI on a landslide, showed that water infiltrating to bedrock took 5 hours to travel 5 meters down (1 m/h), while the wetting front took 12-15 hours to arrive. Preferential flow velocities in karst terrain can be estimated from the ERI tomograms of Carriere et al. (2016) as ~1-10 m/h. Karst terrain can exhibit velocities even higher than ours, for instance Einsiedl (2005) showed tracer breakthrough 1450 m downgradient at 8 hours, which equates to roughly 180 m/h. Yet our velocity estimates are in reality underestimated, with true values being even greater given that our surveys were conducted hourly (thus transit times are overestimated) and flowpaths may be non-vertical and tortuous (thus flowpath lengths are underestimated). This further supports our conclusion of elevated infiltration velocities. On the other hand, field data from coal-mine rock dumps in Canada showed lower transit velocities, in the range of meters per year (Barbour et al. 2016). But there, flow traversed predominantly silts and sands, and thus probably represents mostly matrix-flow dominated flow. Accordingly, these rates are at minimum two orders of magnitude slower than we observed. Neither our approach in this study to evaluate preferential flow, nor methods employed in other studies to evaluate matrix-dominated flow, have been applied to estimate relative flow volumes occurring via these differing processes. This area is ripe for further study. Spatial scale should also be considered, with our fills being comparatively small (200 m up to ~1 km across) relative to waste rock dumps or fills in other regions (multiple km across) (Barbour et al. 2016). Flow velocities in matrix or preferential flowpaths are probably not much influenced by fill size, but rather by fragment sizes and distribution within mined landscapes. Yet migration times across larger fills are likely substantially greater.

The time-lapse tomograms of Office Fill, Bearwallow, and Barton Hollow fills (Figures 4-3 through 4-6) all seem to roughly agree with the corresponding sections of the long dry ERI surveys (Figure 4-1). Regions that displayed low resistivity (blue) on the long dry surveys and may have been fine-grained enough to hold small amounts of antecedent moisture often were also blue in the time-lapse tomograms, suggesting that water accumulated there. Regions of high resistivity (red) in the long dry surveys usually corresponded with the yellow-red inversion artifacts in the time-lapse surveys, which were not getting any wetter. However, the tomograms of End Fill did not seem to agree in this way. The regions of increasing conductivity and inversion artifacts found in the time-lapse tomograms suggest much fewer large, consistent regions are in the subsurface than the long dry survey results would otherwise imply. The consistency between our two types of tomograms in all but one fill suggests that our field and interpretation methods are useful but would benefit from additional refinement.

4.1.2.2 Applied significance for fill construction and monitoring

It would be impractical to significantly rebuild established, conventionally built fills, but it may be worth investigating if relatively minor changes could have comparatively large effects. For example, if the shallow compaction layer within the Barton Hollow experimental fill was the key factor behind reduced infiltration and lowered SC, perhaps there is potential to create such a compaction layer on the top of existing fills or part of existing fills for similar effects. Even this

effort would be substantial, but easier to apply to younger fills where vegetation is less re-established. ERI could be conducted before and after such applications to determine the net effect of both vegetation clearing and compaction on flowpaths and SC.

The knowledge gained from this study can also inform the design and construction of future fills. For the most part, water flow patterns are not considered during fill design and construction beyond ensuring sufficient drainage for geotechnical stability. The subsurface water flow and accumulation patterns observed in this study exhibited wide variation among fills, and the behavior of the water influences the release of TDS from spoils, which leads to variation in effluent SC levels. The study results highlight the need for more intentional fill design and construction methods that incorporate the effect of water flow patterns on water quality.

If more mine sites adopt the thin-lift with compaction approach, the corresponding effluent stream quality may well improve as a result. Furthermore, the construction of additional fills using the Zipper et al. (2015) construction guidelines would allow future studies to determine the variability of flowpaths among such fills. Daniels et al. (2016) tested SC levels over time as a result of leaching in a lab column and found that SC levels started out high and then dropped and stabilized fairly quickly. Field measurements have shown the same trend in valley fill effluent streams, but on a much slower scale of years (Evans et al. 2014, Daniels et al. 2016).

Because infiltration of water along preferential infiltration flowpaths in valley fills can be very fast, yet accumulations of water within the fill occur on longer timescales, it would be beneficial to conduct paired rainfall and effluent flow/SC monitoring at high temporal resolution at a series of fills to hopefully better understand the relationship between rainfall events, flowpath activation, and flow/SC response in the effluent stream. Finally, if more experimental fills were constructed, monitoring their effluent streams would provide valuable feedback on the efficacy of those construction methods.

4.1.2.3 Limitations and future study

The ERI methods employed in this study are beneficial because they are far less invasive than conventional methods such as borings and excavations, and because they produce continuous two-dimensional data rather than point data. Nevertheless, the results are more uncertain than direct physical methods in that we do not directly observe the subsurface (see also Verification work, in Section 4.2 below). There is uncertainty in the data themselves, particularly on the edges of a tomogram. Furthermore, even in regions that displayed water accumulation with high confidence, we cannot quantify how much of the imaged wetness came from our artificial rainfall experiments and how much from water already in the vadose zone.

One of the major challenges of ERI is the tradeoff between survey dimensions and resolution. A long survey's tomogram will cover greater length and depth, but the spatial resolution of the data will be lower than a shorter survey. To increase data resolution over a long survey, it is possible to decrease electrode spacing with a roll-along survey, which is performed one ERI cable at a time, but this limits the depth of the data obtained proportionally to the length of a single survey within the roll-along sequence. For this reason, we opted not to perform any roll-along surveys. Furthermore, ERI is not instantaneous; our 64-electrode surveys took approximately 33 minutes and our 32-electrode surveys 8 minutes, during which the subsurface may have changed, particularly during artificial rainfall. Thus, the temporal resolution of our results has limits.

There are practical concerns with the equipment we used; the ERI equipment is more fragile than many conventional investigation methods, which do not include electrical circuits or sensitive cables. In our case this had the practical effect of reducing the number of cables we were able to use at one of the fills, reducing the tomograms' spatial resolution. The artificial rainfall system in this study was somewhat inconsistent, as the sprinklers were prone to clogging with sediment or organic material, and water pressure varied based on the positioning of the pump in relation to the sprinklers. If we were to repeat this study, we would try to ensure greater consistency of the artificial rainfall system so that each rainfall plot received more uniform sprinkling over space and time and among fills. This could be achieved by using another type of filter on the water pump intake to prevent sprinkler screen clogging. Another limitation of our approach is that the SC of the artificial rainfall varied among fills (Table 3-3). This variation may have had a minor effect on the ERI results in comparison to the effect of the increased subsurface saturation.

Future studies using ERI on other reclaimed surface coal mines would ideally perform both dry and sequential wet surveys on a conventional, i.e. loose dump, fill and an experimentally planned and constructed fill that are otherwise similar over all basic fill characteristics. This would all but eliminate variables such as fill size, drainage basin size, fill age measured since revegetation, land cover, and underlying geology/fill materials, thereby isolating the variable of fill construction method.

4.2 Verification of ERI results

4.2.1 Results

4.2.1.1 Borehole and down-hole video

Drilling started at 9:45 AM on October 24, 2017, and was ended at 3:45 PM at a depth of 17.8 m to allow time to run the video camera before dark. Core samples were collected in 11 drilling runs of approximately 1.5 m each (length of the core tube). However, less than 1.5 m of core was recovered from each run because of collapse of voids and flushing of fines by drilling fluid. Each core was photographed and compared to images captured from the down-hole video (Figure 4-7).

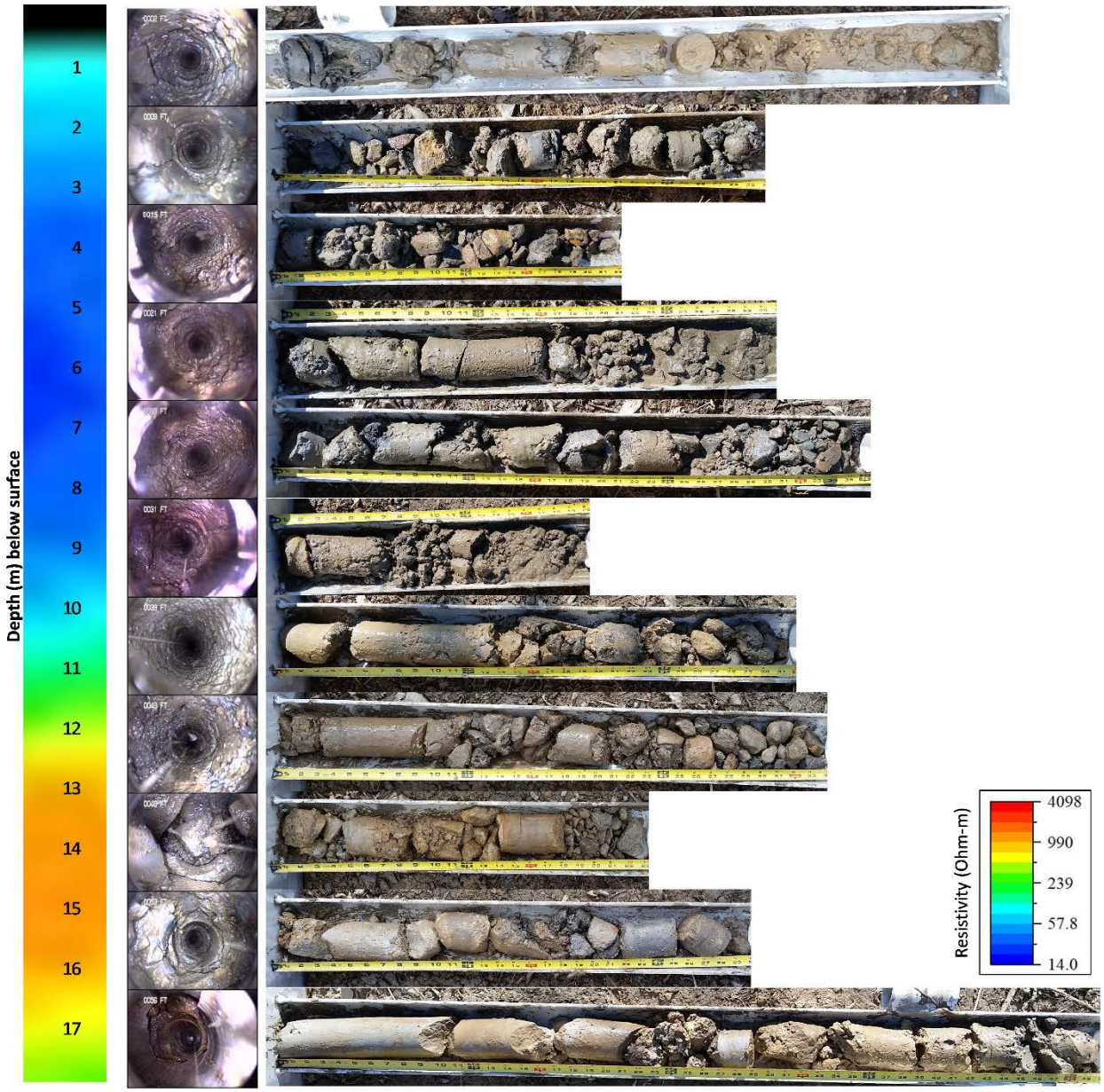

Figure 4-7. Electrical resistivity imaging (ERI) depth profile (left) collected August 20, 2017, along with core samples (right) and video frames (middle) obtained from a 17.8 m vertical borehole drilled October 24, 2017, at Office Fill (Dickenson County, VA). Cores were collected in 11 drilling runs of approximately 1.5 m each. Core samples are shown at an approximately equal scale; thus an image's length is proportional to the amount of material recovered. Video frames look down the borehole from approximately 0.5 m below the top of each 1.5 m drilling run.

General observations of drilling included: 1) after drilling to 12 m the drill operator mentioned that so far the material had been wetter, and had more fines, than expected for loose-dumped rock; 2) cores from below 13 m were drier and had less mud and fines than cores from higher up; 3) when the borehole reached approximately 15 m, return flow (to the surface) of drilling fluid ceased, indicating that the fluid was infiltrating at depth rather than being forced

back up to the surface. Observations from the six video takes follow:

1. In Take 1, the camera was lowered to the bottom of the borehole then raised to 16 m while recording. The dominant material observed was boulders with minimal fines. No seepage of water into the hole from the sides was observed. The material appeared to be well drained.
2. Take 2 was recorded at 14 m. When the first casing section was removed after Take 1, the hole collapsed below 14 m, so no video was recorded at 14–16 m. The material visible on the sides of the hole at 14 m appeared as described in Take 1.
3. Video was recorded from 13.1 to 9.4 m. As the camera rose, the sides of the hole appeared to be increasingly saturated (more water seeping in), and more fines sloughed into the hole, especially above 12 m.
4. Video was recorded from 9.4 to 7.3 m. This section appeared to be very saturated (heavy seepage).
5. Video was recorded from 7.3 to 4 m. Seepage decreased above approximately 4.6 m.
6. Video was recorded from 4 m to the surface. Seepage and sloughing were further reduced, indicating drier material.

4.2.1.2 Artificial rainfall with tracer

The fluorometer was deployed in the effluent stream for 11 days following the October 20, 2017 RWT application. The RWT baseline remained stable throughout the deployment. A RWT method detection limit (MDL) of 1.095 µg/L was calculated from the *in situ* blank RWT readings on days 1–2 (mean = -0.49 µg/L, SD = 0.365 µg/L, n = 288). RWT spiked to 8 µg/L following a 4.2 cm rain on October 23 and to 3 µg/L following a 2.6 cm rain on October 28 (Figure 4-8 top). After excluding RWT data points < MDL and those where turbidity interference (up to 550 NTU on October 23 and 200 NTU on October 28) exceeded the RWT signal, the total mass of RWT discharged was 0.086 g (0.06% of the RWT applied). In case turbidity masked actual RWT discharge, we recalculated RWT mass without accounting for turbidity interference and found the upper limit of RWT discharged to be 0.22 g (0.16% of applied RWT). Therefore at least 99.84% of the applied RWT remained in the valley fill during the October monitoring period.

The entire RWT baseline fluctuated up to 3 µg/L on October 24–25 in the absence of turbidity. This could be interpreted as discharge of a trace amount of RWT, or it could be viewed as baseline interference from an unknown source. Since these “peaks” were so low, and since <0.2% of the applied RWT was recovered, the data are inclusive regarding whether the October 24–25 values represent actual RWT discharged.

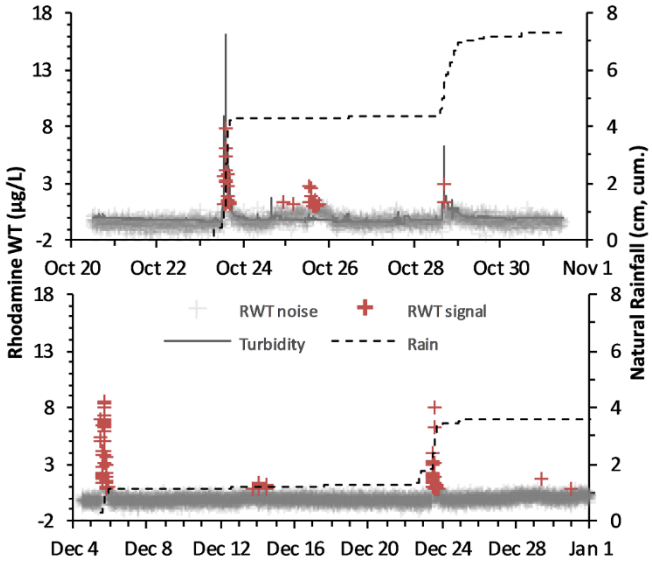

Figure 4-8. Rhodamine WT (RWT) signal (>method detection limit, MDL) and noise (<MDL) detected by a fluorometer in the valley-fill effluent stream following RWT application to the valley-fill surface: in artificial rainfall on October 20, 2017, at End Fill, with turbidity interference expressed as (NTU × 0.03) µg/L apparent RWT (top); and on December 5, 2017, at End Fill, prior to natural rainfall (bottom).

4.2.1.3 Soil pits and infiltration

Stations 1 and 2 at Office Fill had similar soil profiles (Figure 4-9ab). Dense, clayey soil 60 cm thick overlaid rock spoils (sandstone boulders and cobbles) with large (10–40 cm) interstitial voids. The 'A' horizon extended 15–20 cm down from the surface. The upper 60 cm of soil displayed one to two discontinuous horizontal yellowish zones. At Station 1 roots were sparse and fine and largely confined to the upper 20 cm. At Station 2 roots were more abundant, had larger diameter, and were found throughout the upper 60 cm, with many emerging at depths of 50–60 cm. Puddles remained on the surface at Station 1 the day after sprinkling.

At the four plots on End Fill the blue dye typically infiltrated the soil matrix to a depth of 8–18 cm within two hours (4–9 cm/h). Several flowpaths extended along rocks and roots to a depth of 30–38 cm (15–19 cm/h) (Figure 4-9c).

Figure 4-9. Soil pits on valley fills: Office Fill stations 1 (a) and 2 (b); End Fill pit with blue dye flow path around cobbles (c).

4.2.2 Discussion

4.2.2.1 Borehole and downhole video

Observations from down-hole video and inspection of cores at Office Fill (Figure 4-7) were consistent with the ERI tomogram (Figure 4-7, Figure 4-1a at 143 horizontal meters), which showed resistivity varied along a gradient from a maximum at approximately 14 m and minimum at 6 m below the surface. Results of ERI and drilling confirmed our more general conception of valley fill geology/hydrology, including: 1) smaller rocks with more fines near the surface and larger rocks with larger voids at depth; 2) more water storage in the finer sediment at the top; 3) preferential flow through the finer sediment at the top (the boring did not necessary directly confirm this, but it must be so given how quickly water penetrated deeper in the fill from the ERI time lapse during artificial rainfall).

4.2.2.2 Artificial rainfall with tracer

The artificial rainfall RWT tracer exercise did not provide useful data for interpreting rainfall infiltration pathways and their relatively timing and importance during storm events. This occurred for two reasons. First, the tracer was retained to far greater extent than anticipated, such that far greater than 99% of the tracer remained in the fill rather than emerging in the effluent stream. It is possible that this result occurred because the tracer was sorbed to fill material; it is also possible that typical transit times for infiltration waters were greater than the 11-day artificial rainfall monitoring period. For this reason, the RWT peaks seen in the effluent stream could not be interpreted as peaks of flow coming from the fill, because they were so small that they could not be sufficiently distinguished from the noise. Second, RWT sensing suffers from turbidity interference, which contributed to our inability to interpret our data. While this was disappointing, we recognize that these methods had not been attempted before in mine settings (to our knowledge), and as a result, useful knowledge was gained that may be applied to future efforts of this kind. Recommendations include using tracers that sorb less and suffer from less interference with turbidity. The downside of this recommendation is that tracer may be more costly.

4.2.2.3 Soil pits and infiltration

Observations from soil pits and infiltration studies corroborated ERI interpretations. At Office Fill, a series of ERI runs during artificial rainfall showed increasing conductivity (wetting) 1.5–3 m below the surface at stations 1 and 2 (Figure 4-3, 32-39 and 23 horizontal meters, respectively), which we interpreted as evidence of near-surface preferential flowpaths through which rainfall rapidly infiltrated. The soil pits revealed possible flowpaths in the form of voids between rocks at both stations 1 and 2. Although we did not find obvious flowpaths through the upper 60 cm of soil overlaying the rocky fill material, the 5+ cm of artificial rainfall sprinkled during a 4 hour period produced no surface runoff, indicating high permeability.

Although Office Fill Stations 1 and 2 had similar soil profiles and both had large voids in the rocky fill material, ERI at Station 2 showed lower initial (pre-sprinkling) conductivity and a greater percent increase in conductivity during sprinkling than at Station 1 (Figure 4-3, 32-39 horizontal meters). These ERI findings suggest that Station 2 (Figure 4-3, 23 horizontal meters) was better drained than Station 1. Our observations of a deeper, more developed root network at Station 2 and puddles remaining the day after sprinkling at Station 1 support this interpretation of ERI tomograms. The observed differences in moisture retention may reflect the contrasting

topographic positions of Station 1 (flat lift) and Station 2 (steep hillslope) or greater compaction of fill material on the lift during valley fill construction.

ERI tomograms for End Fill showed a zone of increasing conductivity (wetness) developing at a depth of 6+ m within 1 hour of the onset of artificial rainfall (Figure 4-4 at 24-41 horizontal meters) (infiltration rate of 600 cm/h). By sprinkling blue dye and excavating soil pits at End Fill (at 24, 32, 35 and 41 m), we found flowpaths with infiltration rates of up to 19 cm/h, but we expect infiltration occurs much more rapidly in the interstitial voids in the rocky core of the valley fill than in the soil near the surface where we excavated.

4.3 Monitoring Streams and Natural Rainfall Events

4.3.1 Results

4.3.1.1 Effluent stream monitoring

Monitoring began May 1 2017 at all four valley-fill streams and ended October 3, 2017, (end of ERI season) at Barton Hollow, Office Fill, and Bearwallow, but continued until December 31, 2017, at End Fill during RWT monitoring. Some of these data are plotted in Appendix D. During the ERI season (May 24– October 3), median (25%–75%) SC was 1807 µS/cm (1706–1836 µS/cm) at Barton Hollow, 2034 µS/cm (1887–2118 µS/cm) at End Fill, 2268 µS/cm (2087–2361 µS/cm) at Bearwallow, and 2608 µS/cm (2532–2701 µS/cm) at Office Fill. Median (25%–75%) water temperature was 15.2 °C (15.0–15.4 °C) at Barton Hollow, 15.3°C (14.8–15.7 °C) at End Fill, 17.3 °C (16.2–17.8 °C) at Office Fill, and 18.2 °C (17.1–19.7 °C) at Bearwallow. SC data were markedly non-normally distributed for some fills, which is why we present median and interquartile ranges rather than mean and standard deviation. The SC and temperature data series were 100% complete (no missing values) during the ERI season at End Fill. The Barton Hollow, Office Fill, and Bearwallow data series were 78%, 67%, and 51% complete, respectively, because the EC sensor was dewatered (Bearwallow after August 23, Barton Hollow August 11–September 8), a data file was corrupt (Bearwallow, July 10–31), or the EC sensor was buried in sediment (occurred at Office Fill during storms because of an eroding road crossing upstream).

Total rainfall during the ERI season was 37.1 cm at Barton Hollow, 37.2 cm at End Fill, 44.1 cm at Office Fill, and 46.3 cm at Bearwallow (mean = 41.2 cm). Monthly rainfall averaged across all four rain gages was 10 cm in June 2017, 18 cm in July, 7.9 cm in August, 2.7 cm in September, 15.2 cm in October, 4.0 cm in November, and 3.6 cm in December (measured at End Fill only). The greatest 2-day rainfall (12.6 cm) occurred at Bearwallow July 27–28. Other storms producing >4 cm of rain included May 24–25, June 4–5, July 13–14, July 23–24, October 8–9, and October 23. All gages recorded ≤1 mm of rain during September 15–October 7.

Median (25%–75%) *Q* during the ERI season was 0 L/s (0–0.1 L/s) at Bearwallow, 2.7 L/s (1.5–4.9 L/s) at Barton Hollow, 3.5 L/s (2.9–4.5 L/s) at End Fill, and 13.0 L/s (12.7–13.3 L/s) at Office Fill. The End Fill and Barton Hollow *Q* data series were 100% complete. The Bearwallow and Office Fill *Q* data series were 74% and 52% complete, respectively, because a data file was corrupt (Bearwallow, June 6–July 10) or the flume was buried in sediment or bypassed during storms (Office Fill prior to August 1). The Bearwallow flume was dry for 55% of the data points during the ERI season (mostly after August 23), during which *Q* was recorded as 0 L/s.

Median (min–max) monthly (June–September) unit-Q as % of rainfall (Q_R) was 1.9% (0.1–2.9%) at Bearwallow, 22% (10–47%) at Barton Hollow, 34% (21–147%) at End Fill, and 189% (94%–283%) at Office Fill (Table 4-4, Figure 4-10). Q_R was typically greatest in September, which was the driest month.

Table 4-4. Water balance for valley-fill effluent streams.

	Q_U (unit Q, m^3/ha)				Q_R (Q_U as % of m^3/ha of rainfall)				Q_{VF} ($Q_R \times A_{VF}/A_W$, %)			
Month	EF	BH	BW	OF	EF	BH	BW	OF	EF	BH	BW	OF
June	334	213	-	-	35	32	-	-	1.7	4.2	-	-
July	317	209	54	-	21	11	2.9	-	1.0	1.4	1.7	-
August	271	89	8	897	33	10	1.9	94	1.6	1.3	1.1	6.3
Sept-ember	336	103	0.21	801	147	47	0.1	283	7.3	6.2	0.1	19.1
Min	271	89	0.21	801	21	10	0.10	94	1.0	1.3	0.1	6.3
Media n	326	156	8.3	849	34	22	1.9	189	1.7	2.8	1.1	13
Max	336	213	54	897	147	47	2.9	283	7.3	6.2	1.7	19

Valley-fill name (area of valley fill footprint, A_{VF}, area contributing to flume watershed, A_W): EF = End Fill (1.5 ha, 30.35 ha), BH = Barton Hollow (7.0 ha, 53.26 ha), BW = Bearwallow (15 ha, 25.30 ha), OF = Office Fill (2.8 ha, 41.52 ha). "-" indicates missing discharge data.

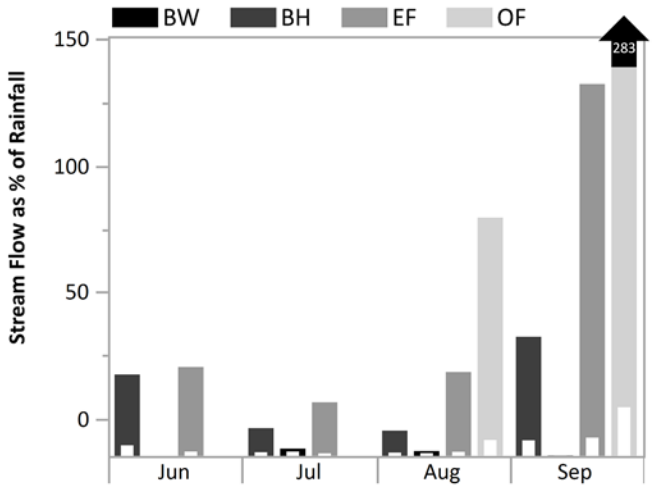

Figure 4-10. Water balance for valley-fill effluent streams. Main bars indicate monthly unit discharge as a percentage of rainfall volume (Q_R). Nested white bars indicate the fraction of stream flow originating as rainfall on the valley-fill footprint (Q_{VF}). Bearwallow was missing discharge data for June 2017. Office Fill was missing discharge data for June and July. Abbreviations defined in Table 4-4 footnote.

Median (min–max) monthly (June–September) rainfall volume on a valley fill as % of Q was 5% (2–7%) at Office Fill, 15% (3–24%) at End Fill, 79% (28–136%) at Barton Hollow, and 3,163% (2,078–96,001%) at Bearwallow (Table 4-5). SC–Q bivariate plots for individual rain

events showed hysteresis with clockwise rotation at Office Fill, End Fill, and Bearwallow, and counterclockwise rotation at Barton Hollow (Figure 4-11).

Table 4-5. Volume of rainfall on valley fill footprint as a percent of effluent stream discharge.

	Rainfall on valley fill as % of *Q*			
Month	EF	BH	BW	OF
June	14%	42%	-	-
July	24%	117%	2078%	-
August	15%	136%	3163%	7%
September	3%	28%	96001%	2%
Min	3%	28%	2078%	2%
Median	15%	79%	3163%	5%
Max	24%	136%	96001%	7%

Abbreviations as defined in the Table 4-4 footnote. Rainfall volume estimated based on rain gage data and area of valley-fill footprint estimated using Google Earth.

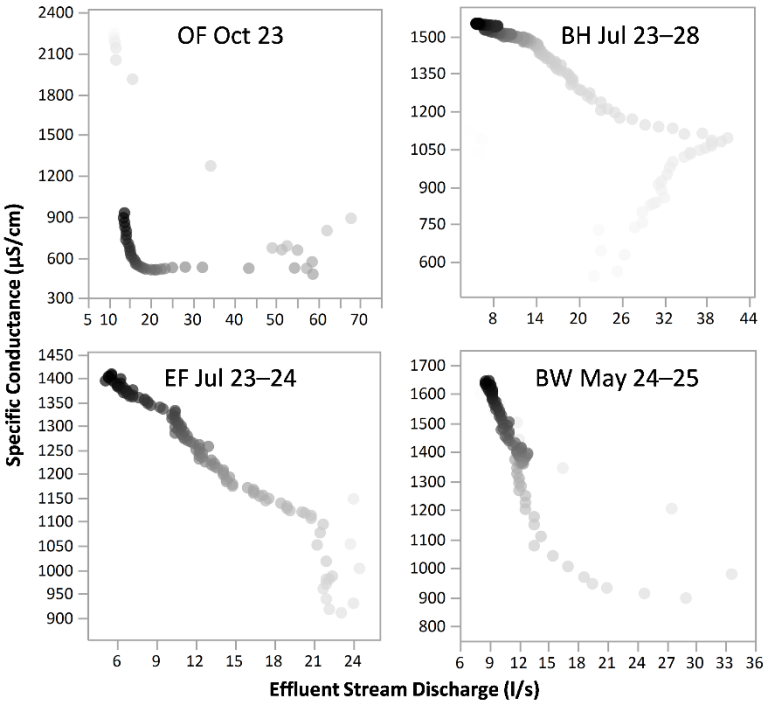

Figure 4-11. Examples of SC–Q bivariate plots showing hysteresis for individual rain events with clockwise rotation (OF, EF, BW) and counterclockwise rotation (BH). Darker-shaded bubbles were recorded later in time. Abbreviations as defined in the Table 4-4 footnote.

4.3.1.2 Natural rainfall with tracer

RWT was applied December 4, 2017. It rained 1.2 cm on December 5 and 2.3 cm on December 23. RWT concentration was monitored in the valley fill effluent stream through January 1 (28 days). The fluorometer's temperature compensation malfunctioned, so the raw

RWT concentration readings fluctuated synchronously with water temperature (r = 0.945). To remove the variability in RWT readings attributable to water temperature, we regressed the raw RWT readings against water temperature and used the residuals as corrected RWT readings. The residuals were rescaled (multiplied by 0.85) such that the average of the first two readings (taken in RWT calibration solution) matched the known concentration (20 µg/L) of the calibration solution. A RWT MDL of 0.786 µg/L was calculated from a representative 2-day portion of the baseline (mean = -0.159 µg/L, SD = 0.262 µg/L, n = 288).

As with the artificial rainfall experiment, RWT readings briefly spiked to 8–9 µg/L following rains on December 5 and 23 (Figure 4-8 bottom). A turbidity sensor was not deployed in December; however, assuming an equivalent response of turbidity to rainfall in December as was measured in October, turbidity interference probably explained little of the December 4 RWT signal but most of the December 23 RWT signal. Up to 0.375 g of RWT (without accounting for turbidity interference) was discharged (0.007% of the 5,606 g applied); therefore, ≥ 99.993% of the applied RWT remained in the valley fill during the December monitoring period.

4.3.2 Discussion

4.3.2.1 Effluent stream monitoring

Baseflow at Office Fill was noticeably higher and less variable than at End Fill and Barton Hollow, and unit-Q at Office Fill was also comparatively elevated. This may reflect input from an underground mine (unverified). Frequent flume dewatering and low unit-Q at Bearwallow (Table 4-4) may be explained by a low water table (subsurface flow) attributable to the stream channel being constructed on porous fill material. Inter-watershed transfer via ditches may also have contributed to observed differences in unit-Q between watersheds. Q_R was typically greatest in September, which was the driest month. The most plausible explanation is release of water stored in the valley fills (perhaps augmented by ongoing deep-mine discharge at Office Fill).

We attribute reduced SC at Barton Hollow to experimental valley fill construction practices designed to minimize discharged TDS (Zipper et al. 2015). Barton Hollow was also recently revegetated (fall 2015), so SC may continue to rise. Typically SC peaks 3 years after valley fill revegetation (Evans et al. 2014).

Precipitation as a percentage of effluent stream flow was greatest at Bearwallow due to lowest flow among the fills (Table 4-5). Conversely, precipitation as a percentage of effluent stream flow was lowest at Office Fill due to high effluent flow and low fill area.

SC–Q bivariate plots for individual rain events showed hysteresis with clockwise rotation at Office Fill, End Fill, and Bearwallow, and counterclockwise rotation at Barton Hollow (Figure 4-11). Clockwise rotations indicate a rise in SC followed by a rise in Q, indicating a first flush of TDS that may accumulate on the soil surface or along preferential flowpaths within the fill (Clark et al. 2016). Counterclockwise rotations indicate the opposite pattern, with a rise in Q followed by a rise in SC. This implies dilute water being mobilized first, which can occur during larger storms or where infiltration capacity of the valley fill surface is comparatively low (Clark et al. 2016).

4.3.2.2 Natural rainfall with tracer

The natural rainfall RWT tracer exercise did not provide useful data for interpreting rainfall infiltration pathways and their relatively timing and importance during storm events. This occurred for two reasons. First, the tracer was retained to far greater extent than anticipated, such that far greater than 99% of the tracer remained in the fill rather than emerging in the effluent stream. It is possible that this result occurred because the tracer was sorbed to fill material; it is also possible that typical transit times for infiltration waters were greater than the 28-day natural rainfall monitoring period. For this reason, the RWT peaks seen in the effluent stream could not be interpreted as peaks of flow coming from the fill, because they were so small that they could not be sufficiently distinguished from the noise. Second, RWT sensing suffers from turbidity interference, which contributed to our inability to interpret our data. While this was disappointing, we recognize that these methods had not been attempted before in mine settings (to our knowledge), and as a result, useful knowledge was gained that may be applied to future efforts of this kind. Recommendations include using tracers that sorb less and suffer from less interference with turbidity. The downside of this recommendation is that tracer may be more costly.

4.4 Relating Valley Fill Geology with Effluent Hydrology and Water Quality

We performed various linear regressions with fill properties and flowpath properties (Appendix C). However, this analysis did not result in a compelling outcome; all but one R^2 value were below 0.5, and all were below 0.6. Although our sample size was small, there were no strong correlations between any two of the variables we analyzed when all flowpaths and fills were considered.

Regressions of quantifiable fill and flowpath properties did not reveal any statistically significant patterns among all the valley fills. Some fill properties, such as age since reclamation and vegetation, are understood to affect infiltration and subsurface flow, although vegetation's influence is only relevant within about a meter of the surface (Evans et al. 2015). For example, Ritter and Gardner (1993) found that young fills in Pennsylvania had low infiltration rates, but over a twelve-year study most of their sites' infiltration capacities increased, possibly due to vegetation growth. Similarly, Guebert and Gardner (2001) observed low infiltration capacities on recently reclaimed lands, but two years later they found that vegetation growth had helped to create macropores and increase infiltration. The variability within these general patterns remains such that flowpath development cannot be predicted well (Evans et al. 2015).

5. CONCLUSION

Here we summarize how the project addressed the Objectives laid out in the Introduction (Section 1).

5.1 Map Hydrologic Flowpaths through Valley Fills (Objective 1)

We found a significant amount of variation in subsurface structure in the electrical resistivity imaging (ERI) tomograms of our four field sites. One of the most visible differences among fills was that the experimentally constructed Barton Hollow had a relatively small range of resistivity compared to the three conventionally constructed fills, suggesting more consistent internal structure throughout the fill. Using time-lapse ERI surveys, we were able to identify a total of eight deep accumulation zones beneath the artificial rainfall plots across the four fills. We observed fewer of these accumulation zones at Barton Hollow than at the other three fills, suggesting that the internal structure of the fill helps keep water infiltration shallow.

Our study confirms the usefulness of ERI as a noninvasive tool for hydrogeologic analysis of valley fills, as it is able to image internal structure under dry conditions and subsurface flowpaths under rainfall conditions. Our results suggest that the intentionally planned structure of valley fills may help control infiltration to the deep bulk fill and thereby improve effluent water quality.

5.2 Determine Residence Times of Flowpaths (Objective 2)

Based on the identified accumulation zones, we estimated an average flowpath transit time of 1.4 hours, average length of 6.6 meters, and average velocity of ≥5.1 m/h or ≥0.14 cm/s. These transit time and velocity values indicate faster infiltration than that observed on many natural lands. These velocities are likely underestimates due to our measurement methods, such that the true velocities are likely higher.

5.3 Determine How Flowpath Location and Residence Time Control Contribution to Effluent Water Quality (Objective 3)

Baseflow at Office Fill was noticeably higher and less variable than at End Fill and Barton Hollow, possibly due to input from an underground mine. Comparatively low flow at Bearwallow may be due to a low water table due to stream channel construction with porous fill material. Precipitation as a percentage of effluent stream flow was accordingly greatest at Bearwallow and lowest at Office Fill.

Average specific conductance (SC) was lowest at Barton Hollow, likely due to experimental valley fill construction practices designed to minimize discharged total dissolved solids (TDS). SC–flow(Q) bivariate plots for individual rain events showed hysteresis with clockwise rotation at Office Fill, End Fill, and Bearwallow, and counterclockwise rotation at Barton Hollow. Clockwise rotations indicate a first flush of TDS that may accumulate on the soil surface or along preferential flowpaths within the fill, while counterclockwise rotations may indicate lower infiltration capacity.

Neither the rhodamine WT tracer (RWT) exercise with artificial rainfall nor that with natural rainfall provided data that were useful in interpreting valley fill hydrology because of

greater sorption of tracer to fill soils and/or transit times than expected (such that greater than 99% of the tracer remained in the fill rather than emerging in the effluent stream) and RWT sensor interference from turbidity. Yet this experience provided lessons learned that can inform future efforts.

5.4 Determine How Contribution to Effluent Water Quality is Controlled by Fill Characteristics (Objective 4)

Regressions of quantifiable fill (such as fill age, construction method, and reclamation method) and flowpath (such as length, transit time, velocity) properties did not reveal any statistically significant relationships. Thus, we are unable to assert that the age, fill size, or drainage basin size of a fill affects the preferential infiltration flowpath lengths, transit times, or flow velocities observed there. We also did not find any statistically significant patterns between fill or flowpath properties and effluent streams' SC when we included all four valley fills in our regression. Removing Barton Hollow from that analysis revealed a negative correlation between fill age and SC, suggesting that younger fills typically contribute higher levels of TDS to their effluent streams but that Barton Hollow's experimental construction method and associated altered flow patterns may help keep its effluent stream's SC low. The finding that effluent streams of younger fills have higher SC's is consistent with findings of a prior study (Evans et al. 2014).

5.5 Independently Verify Hydrogeologic Interpretations of ERI Results (Objective 5)

The RWT tracer exercise with artificial rainfall did not provide data that were useful in interpreting valley fill hydrology because of greater sorption of tracer to fill soils than expected (such that greater than 99% of the tracer remained in the fill rather than emerging in the effluent stream) and RWT sensor interference from turbidity. Yet this experience provided lessons learned that can inform future efforts.

Observations from soil pits and infiltration studies successfully corroborated ERI interpretations. At both Office Fill and End Fill, soil pits revealed possible preferential flowpaths in the form of voids between rocks that are consistent with ERI tomograms during artificial rainfall showing increasing conductivity (wetting) beneath.

Observations from down-hole video and inspection of cores at Office Fill also successfully verified ERI interpretations. This work confirms that 1) smaller rocks with more fines were found near the surface of the valley fill and larger rocks with larger voids were found at depth; 2) more water was stored in the finer sediment at the surface of the valley fill; and 3) preferential occurs flow must be occurring through finer sediment at the surface of the valley fill.

6. REFERENCES

AGI. 2009. Instruction Manual for EarthImager 2D Version 2.4.0 Resistivity and IP Inversion Software. Advanced Geosciences, Inc. Austin, TX, USA.

AGI. 2017 SuperStingTM Earth Resistivity, IP & SP System With Wi-Fi® Instruction Manual. Retrieved January 20, 2018, from http://www.advancedgeosciences.com/files/cust/superstinguser.shtml.

Agouridis, C. T., P. N. Angel, T. J. Taylor, C. D. Barton, R. C. Warner, X. Yu, and C. Wood. 2012. Water Quality Characteristics of Discharge from Reforested Loose-Dumped Mine Spoil in Eastern Kentucky. Journal of Environmental Quality **41**:454-468.

Barbour, S. L., M. J. Hendry, and S. K. Carey. 2016. High-resolution profiling of the stable isotopes of water in unsaturated coal waste rock. Journal of Hydrology **534**:616-629.

Carriere, S. D., K. Chalikakis, C. Danquigny, H. Davi, N. Mazzilli, C. Ollivier, and C. Emblanch. 2016. The role of porous matrix in water flow regulation within a karst unsaturated zone: an integrated hydrogeophysical approach. Hydrogeology Journal **24**:1905-1918.

Caruccio, F. T., and G. Geidel. 1984. Induced alkaline recharge zones to mitigate acidic seeps. Proceedings of the Symposium on Surface Mining, Hydrology, Sedimentology, and Reclamation, Lexington KY, University of Kentucky.

Clark, E. V., B. M. Greer, C. E. Zipper, and E. T. Hester. 2016. Specific conductance-stage relationships in Appalachian valley fill streams. Environmental Earth Sciences **75**.

Clark, E. V., and C. E. Zipper. 2016. Vegetation influences near-surface hydrological characteristics on a surface coal mine in eastern USA. Catena **139**:241-249.

Cormier, S. M., G. W. Suter, II, and L. Zheng. 2013. Derivation of a benchmark for freshwater ionic strength. Environmental Toxicology and Chemistry **32**:263-271.

Daniels, W. L., Z. W. Orndorff, M. J. Eick, and C. E. Zipper. 2013. Predicting TDS release from Appalachian mine spoils. p. 275 - 285 In: J.R. Craynon (ed.), Proceedings, Environmental Considerations in Energy Production, April 14-18, 2013, Charleston, WV. Society for Mining, Metallurgy, and Exploration, Englewood, CO.

Daniels, W. L., J. M. Parker, Z. W. Orndorff, L. C. Ross, C. E. K. Zipper, S.C., and M. J. Eick. 2015. Further evaluation of a simple column leaching method to predict potential TDS losses from central Appalachian overburden materials. In: J.R. Craynon (ed.), Proceedings, Second Environmental Considerations in Energy Production Conference, September 20-13, 2015, Pittsburgh, PA. Society for Mining, Metallurgy, and Exploration, Englewood, CO.

Daniels, W. L., C. E. Zipper, Z. W. Orndorff, J. Skousen, C. D. Barton, L. M. McDonald, and M. A. Beck. 2016. Predicting total dissolved solids release from central Appalachian coal mine spoils. Environmental Pollution **216**:371-379.

Einsiedl, F. 2005. Flow system dynamics and water storage of a fissured-porous karst aquifer characterized by artificial and environmental tracers. Journal of Hydrology **312**:312-321.

Evans, D., C. Zipper, E. Hester, and S. Schoenholtz. 2015. Hydrologic effects of surface coal mining in Appalachia (USA). Journal of American Water Resources Assoiation **51**:1436-1452.

Evans, D. M., C. E. Zipper, P. F. Donovan, and W. L. Daniels. 2014. Long-term trends of specific conductance in waters discharged by coal-mine valley fills in Central Appalachia, USA. Journal of the American Water Resources Association **50**:1449-1460.

Greer, B. M., T. J. Burbey, C. E. Zipper, and E. T. Hester. 2017. Electrical resistivity imaging of hydrologic flow through surface coal mine valley fills with comparison to other landforms. Hydrological Processes **31**:2244-2260.

Griffith, M. B., S. B. Norton, L. C. Alexander, A. I. Pollard, and S. D. LeDuc. 2012. The effects of mountaintop mines and valley fills on the physicochemical quality of stream ecosystems in the central Appalachians: A review. Science of the Total Environment **417**:1-12.

Guebert, M. D., and T. W. Gardner. 2001. Macropore flow on a reclaimed surface mine: infiltration and hillslope hydrology. Geomorphology **39**:151-169.

Hartman, K. J., M. D. Kaller, J. W. Howell, and J. A. Sweka. 2005. How much do valley fills influence headwater streams? Hydrobiologia **532**:91-102.

Hawkins, J. W. 1998. Hydraullic properties of surface mine spoils of the Northern Appalachian Plateau. Proceedings of the 15th National Meeting of the American Society of Mining and Reclamation, St. Louis, MO.

Hawkins, J. W. 2004. Predictability of Surface Mine Spoil Hydrologic Properties in the Appalachian Plateau. Ground Water **42**:119-125.

Hawkins, J. W., and W. W. Aljoe. 1992. Pseudokarst groundwater hydrologic characteristics of a mine spoil aquifer. Mine Water and the Environment **11**:37-52.

Herman, R. 2001. An introduction to electrical resistivity in geophysics. American Journal of Physics **69**:943-952.

Johnson, T. C., L. D. Slater, D. Ntarlagiannis, F. D. Day-Lewis, and M. Elwaseif. 2012. Monitoring groundwater-surface water interaction using time-series and time-frequency analysis of transient three-dimensional electrical resistivity changes. Water Resources Research **48**.

LaBrecque, D. J., M. Miletto, W. Daily, A. Ramirez, and E. Owen. 1996. The effects of noise on Occam's inversion of resistivity tomography data. Geophysics **61**:538-548.

Langston, G., L. R. Bentley, M. Hayashi, A. McClymont, and A. Pidlisecky. 2011. Internal structure and hydrological functions of an alpine proglacial moraine. Hydrological Processes **25**:2967-2982.

Mack, B., J. Filbert, B. Gutta, and P. Ziemkiewicz. 2013. Natural attenuation of TDS in mountaintop mines. P. 265-274, in: J.R. Craynon (ed.), Proceedings, Environmental Considerations in Energy Production, April 14-18, 2013, Charleston, WV. Society for Mining, Metallurgy, and Exploration, Englewood, CO.

Merricks, T. C. 2003. Ecotoxicological Evaluation of Hollow Fill Drainages in Low Order Streams in the Appalachian Mountains of Virginia and West Virginia (Master's thesis). Available from VTechWorks database. http://hdl.handle.net/10919/32977.

Merricks, T. C., D. S. Cherry, C. E. Zipper, R. J. Currie, and T. W. Valenti. 2007. Coal-mine hollow fill and settling pond influences on headwater streams in southern West Virginia, USA. Environmental Monitoring and Assessment **129**:359-378.

Miller, A. J., and N. P. Zegre. 2014. Mountaintop Removal Mining and Catchment Hydrology. Water **6**:472-499.

Miller, C. R., P. S. Routh, T. R. Brosten, and J. P. McNamara. 2008. Application of time-lapse ERT imaging to watershed characterization. Geophysics **73**:G7-G17.

Mojica, A., I. Díaz, C. A. Ho, F. Ogden, R. Pinzón, J. Fábrega, and J. Hendrickx. 2013. Study of Seasonal Rainfall Infiltration via Time-Lapse Surface Electrical Resistivity Tomography: Case Study of Gamboa Area, Panama Canal Watershed. https//doi.org/10.4137/ASWR.S12306. Air, Soil and Water Research **6**:ASWR.S12306. .

Oldenburg, D. W., and Y. G. Li. 1999. Estimating depth of investigation in dc resistivity and IP surveys. Geophysics **64**:403-416.

Orndorff, Z. W., W. L. Daniels, C. E. Zipper, M. Eick, and M. Beck. 2015. A column evaluation of Appalachian coal mine spoils' temporal leaching behavior. Environmental pollution (Barking, Essex : 1987) **204**:39-47.

Pellicer, X. M., M. Zarroca, and P. Gibson. 2012. Time-lapse resistivity analysis of Quaternary sediments in the Midlands of Ireland. Journal of Applied Geophysics **82**:46-58.

Pond, G. J., M. E. Passmore, F. A. Borsuk, L. Reynolds, and C. J. Rose. 2008. Downstream effects of mountaintop coal mining: comparing biological conditions using family- and genus-level macroinvertebrate bioassessment tools. Journal of the North American Benthological Society **27**:717-737.

Pond, G. J., M. E. Passmore, N. D. Pointon, J. K. Felbinger, C. A. Walker, K. J. G. Krock, J. B. Fulton, and W. L. Nash. 2014. Long-Term Impacts on Macroinvertebrates Downstream of Reclaimed Mountaintop Mining Valley Fills in Central Appalachia. Environmental Management **54**:919-933.

Ritter, J. B., and T. W. Gardner. 1993. Hydrologic evolution of drainage basins disturbed by surfacing mining, Central Pennsylvania. Geological Society of America Bulletin **105**:101-115.

Robinson, A. R., and A. R. Chamberlain. 1960. Trapezoidal flumes for open-channel flow measurement. Transactions of the American Society of Agricultural Engineers **3**:120-128.

Seaton, W. J., and T. J. Burbey. 2002. Evaluation of two-dimensional resistivity methods in a fractured crystalline-rock terrane. Journal of Applied Geophysics **51**:21-41.

Simmons, J. A., W. S. Currie, K. N. Eshleman, K. Kuers, S. Monteleone, T. L. Negley, B. R. Pohlad, and C. L. Thomas. 2008. Forest to reclaimed mine land use change leads to altered ecosystem structure and function. Ecological Applications **18**:104-118.

Smart, P. L., and I. M. S. Laidlaw. 1977. Evaluation of some fluorescent dyes for water tracing. Water Resources Research **13**:15-33.

Teledyne Isco. 2013. Isco open channel flow measurement handbook (7th ed.). Teledyne Isco, Lincoln, NE, USA.

Timpano, A. J., S. H. Schoenholtz, D. J. Soucek, and C. E. Zipper. 2015. Salinity as a limity factor for biological condition in mining-influenced central Appalachian headwater streams. Journal of the American Water Resources Association **51**:240-250.

Travelletti, J., P. Sailhac, J. P. Malet, G. Grandjean, and J. Ponton. 2012. Hydrological response of weathered clay-shale slopes: water infiltration monitoring with time-lapse electrical resistivity tomography. Hydrological Processes **26**:2106-2119.

Trudgill, S. T. 1987. Soil-water dye tracing, with special reference to use of rhodamine-WT, lissamine-ff and amino-g-acid. Hydrological Processes **1**:149-170.

USEPA. 2016. Definition and Procedure for the Determination of the Method Detection Limit, Revision 2 (EPA 821-R-16-006). Washington D.C. Available: https://www.epa.gov/cwa-methods; downloaded Jan 2018.

USGS. 2013. National Elevation Dataset, 1/3 arc-second DEM. Sioux Falls, SD. Available: http://nationalmap.gov (Mar 2013).

Wunsch, D. R., J. S. Dinger, and C. D. R. Graham. 1999. Predicting ground-water movement in large mine spoil areas in the Appalachian Plateau. International Journal of Coal Geology **41**:73-106.

YSI. 2012. 6-Series Multiparameter Water Quality Sondes User Manual. YSI Incorporated, Yellow Springs, OH, USA.

Zipper, C. E., E. V. Clark, W. L. Daniels, and R. J. Krenz. 2015. Mine spoil fill construction for reducing total dissolved solids in discharged waters. In 2nd Environmental Considerations in Energy Production Conference, Crayon, J. R. (Ed.). Pittsburgh, P.A. Englewood, CO: Society for Mining, Metallurgy and Exploration Inc.

7. ACKNOWLEDGEMENTS

This project was primarily supported by US Office of Surface Mining Reclamation and Enforcement, grant number S16AC20076, with matching funds from Virginia Tech and the Wells Fargo Clean Technology and Innovation Grant program. The authors offer thanks to the following parties for their help and cooperation: Lauren Eastes, Dylan Honardoust, and Katherine Santizo for field assistance; Harold E. Post II for rainfall gauges; Jermy Yahya, Jackie Ball, and others at Contura Energy, and Chris Stanley and others at Cambrian Coal for cooperation and site access; Steven Ball, Larry Shores, and Jay Hawkins from OSMRE for field assistance and use of the bore-hole camera; Elyse Clark for advice on soil infiltration methods.

8. APPENDICES

Appendix A – Electrical Resistivity Imaging (ERI) and Artificial Rainfall Field Setup Photographs

Figure A-1: Electrode Setup

Figure A-2: Switch Box Setup

The two passive cables are attached to the switch box on the right, while on the left a cable connects the switch box to the resistivity meter.

Figure A-3: Resistivity Meter Setup
The resistivity meter is connected to the switch box (right) and the marine battery (front).

Figure A-4: Short Transect Setup
Note that the resistivity system setup is under the tarp and in the middle of the transect.

Figure A-5: Water Pump
The intake hose (bottom) draws water from the fill's effluent stream. The outlet hose (top) carries the water up the slope.

Figure A-6: Fire Hose Approaching Transect

Figure A-7: Garden Hose and Sprinkler Setup

The fire hose coming up the hill from the pump flows into a four-way splitter, which directs the water into three garden hoses.

Figure A-8: Intake Hose and Water Tank

At Bearwallow, the effluent stream was not reliable and we pumped water from a tank instead.

Appendix B – Electrical Resistivity Imaging Procedure

The resistivity system used in this study, the SuperSting R8 by Advanced Geosciences, Inc., is an eight-channel resistivity meter used in conjunction with a centralized switch box and passive cables. Before beginning survey setup, it is necessary to know the length of the desired transect in order to determine the appropriate spacing for even electrode placement. Topographical data should also be gathered if the survey is not on flat ground; this information is used in a terrain file during data processing. To set up a survey, the stainless steel electrodes must be hammered into the ground about 0.3 meters, and good contact with the earth should be ensured. The electrodes should be placed in as close to a straight even line as possible, although sometimes obstructions in the subsurface such as rocks may require electrode installation to deviate from the center line. Next, passive ERI cables must be laid out and connected to the electrodes via the metal contact points on the cables. The length of these cables may vary between systems; we used cables that connected to 16 electrodes each. Once the cables are in place, they are connected to the switch box. For a 64-electrode (four-cable) setup, the switch box goes between the second and third passive cables. For a 32-electrode (two-cable) setup, the switch box is placed at the top of the transect and connected to the second cable only. Finally, the switch box connects via short cables to the resistivity meter, which in turn is connected to a 12-volt marine battery for portable power (Figure A-1 through Figure A-4).

Once all the parts are connected, it is suggested to perform a contact resistance test, which is one of the diagnostic test features available on the resistivity meter. It measures the resistance between pairs of consecutive electrodes and provides a measure of the earth-electrode contact. If the resistance is too high (generally >5000 ohms), the connection is considered inadequate and would not produce acceptable results. In these cases, the corresponding electrodes may be improved by relocating them or pouring small amounts of water over them to improve earth-electrode contact. Once all electrode contact resistance values are satisfactory, the ERI survey can be run. We used an automatic survey in this study, meaning that the resistivity meter will run the entire survey based on the specified preprogrammed command file (AGI 2017). For each line of the command file, the resistivity meter will distribute current into the ground through two electrodes, referred to as A and B (Herman 2001, AGI 2017). The potential difference between two other electrodes, referred to as M and N, is recorded. The resistivity meter calculates the apparent resistivity by dividing the observed voltage by the injected current (Herman 2001). Command files may structure the patterns of electrodes for measurement in various ways, known as arrays. We selected a command file structured as a dipole-dipole array, in which electrodes A and B are near each other, and M and N are near each other on the other end of the measurement. Dipole-dipole arrays provide more reliable deep measurements than other arrays (Herman 2001).

Appendix C – Statistical Analysis of Fill and Flowpath Properties

In these regressions (Table C-1) we included all flowpaths estimated from the significant accumulation zones at depth (Table 4-1). We took all fill properties, including mean SC of the fills' effluent streams, from Table 3-1. In all linear regressions not involving SC, we also included accumulation zones from the surveys of Greer et al. (2017) for the sake of increasing the sample size (Table C-2). However, we do not have information about the SC of the Powell River Project site's effluent stream, so the last six regressions include only data from this study. The transit times of more lateral flowpaths are more difficult to distinguish with any degree of accuracy, and therefore we have not included them in this analysis.

Table C-1: Fill and Flowpath Properties Linear Regression Results

Independent Variable	Dependent Variable	R^2
Fill area (ha)	Transit time (h)	0.12
Fill area (ha)	Flowpath length (m)	0.20
Fill area (ha)	Flowpath velocity (m/h)	0.52
Drainage area (ha)	Transit time (h)	0.01
Drainage area (ha)	Flowpath length (m)	0.06
Drainage area (ha)	Flowpath velocity (m/h)	0.01
Age (yr)	Transit time (h)	0.00
Age (yr)	Flowpath length (m)	0.03
Age (yr)	Flowpath velocity (m/h)	0.03
Fill area (ha)	Mean SC (µS/cm)	0.00
Drainage area (ha)	Mean SC (µS/cm)	0.11
Age (yr)	Mean SC (µS/cm)	0.03
Transit time (h)	Mean SC (µS/cm)	0.41
Flowpath length (m)	Mean SC (µS/cm)	0.04
Flowpath velocity (m/h)	Mean SC (µS/cm)	0.15
Time since last rainfall (d)	Flowpath velocity (m/h)	0.50

Table C-2: Preferential Infiltration Flowpath Properties from Powell River Project

Figure in Greer et al. (2017)	Horizontal Location (m)	Time to First Appearance, or Flowpath Transit Time (h)	Approximate Vertical Depth from Surface, or Flowpath Length (m)	Approximate Linear Water Velocity along Flowpath (m/h)
Figure 7	52.5	1.25	10.0	8.0
Figure 7	35	1.25	5.0	4.0
Figure 8	40	0.75	5.5	7.33
Figure 8	50	0.75	5.0	6.67

The data show a slight negative association between flowpath velocity and antecedent moisture conditions (Table 3-3), suggesting that water might infiltrate and flow more slowly in drier earth, but the correlation is not strong enough to be statistically significant.

Notably, when the experimentally constructed Barton Hollow is removed from the data, two apparent correlations appear for the SC of conventionally constructed fills' effluent streams. A negative relationship between SC and fill age since reclamation had an R^2 value of 0.77, and a positive relationship between SC and total drainage area had an R^2 value of 0.61. However, with a sample size of only three conventional fills, these two correlations remain very uncertain but give a sense of which fill characteristics may affect effluent SC. They suggest that younger fills' effluent streams typically have higher levels of TDS, perhaps because the very water-spoil contact that leads to high effluent TDS in general may gradually reduce the TDS contribution potential of the spoils. Barton Hollow's deviation from this pattern suggests that its construction method and observed limited deep infiltration may help maintain a relatively low-TDS effluent even as a young fill. Indeed, Evans et al. (2014) observed declining SC of waters in an analysis of long-term fill effluent monitoring results. However, Merricks (2003), and Clark et al. (2016) did not find a significant relationship between the age and effluent SC of the valley fills they studied. Considered together, these studies suggest that other factors such as subsurface materials and structure affect the effluent water quality, but that any given fill's effluent stream quality will likely improve over time.

Appendix D – Rainfall and Flow Monitoring

The following figures represent ongoing monitoring of the four field sites and their effluent streams. The date range shown is our field season, May 22, 2017 through October 3, 2017. In the legends, BH represents Barton Hollow, BW is Bearwallow, OF is Office Fill, and EF is End Fill.

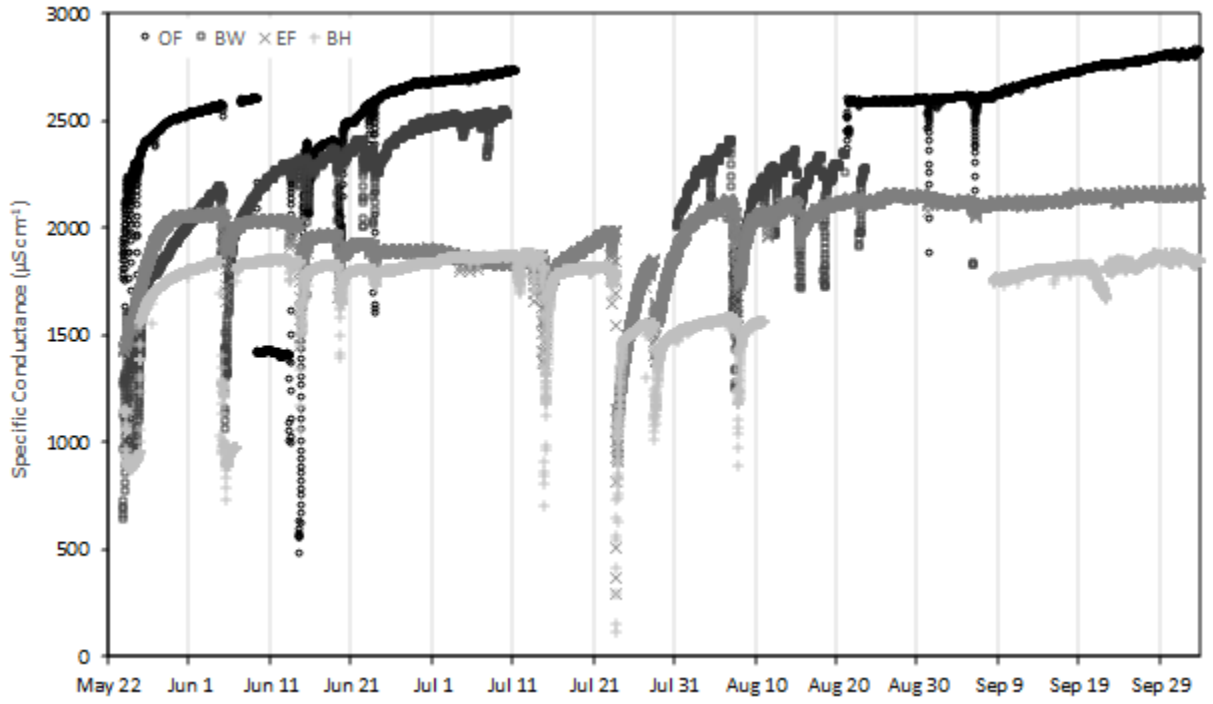

Figure D-1: Specific Conductance during Field Season
The logger sensor at Barton Hollow was dewatered from 08/11/17 – 09/08/17. The data file from Bearwallow from 07/10/17 – 07/31/17 was corrupt. The logger sensor was buried and/or lost at Office Fill from 06/05/17 – 06/07/17, 07/11/17 – 08/21/17, and 10/23/17 – 10/31/17.

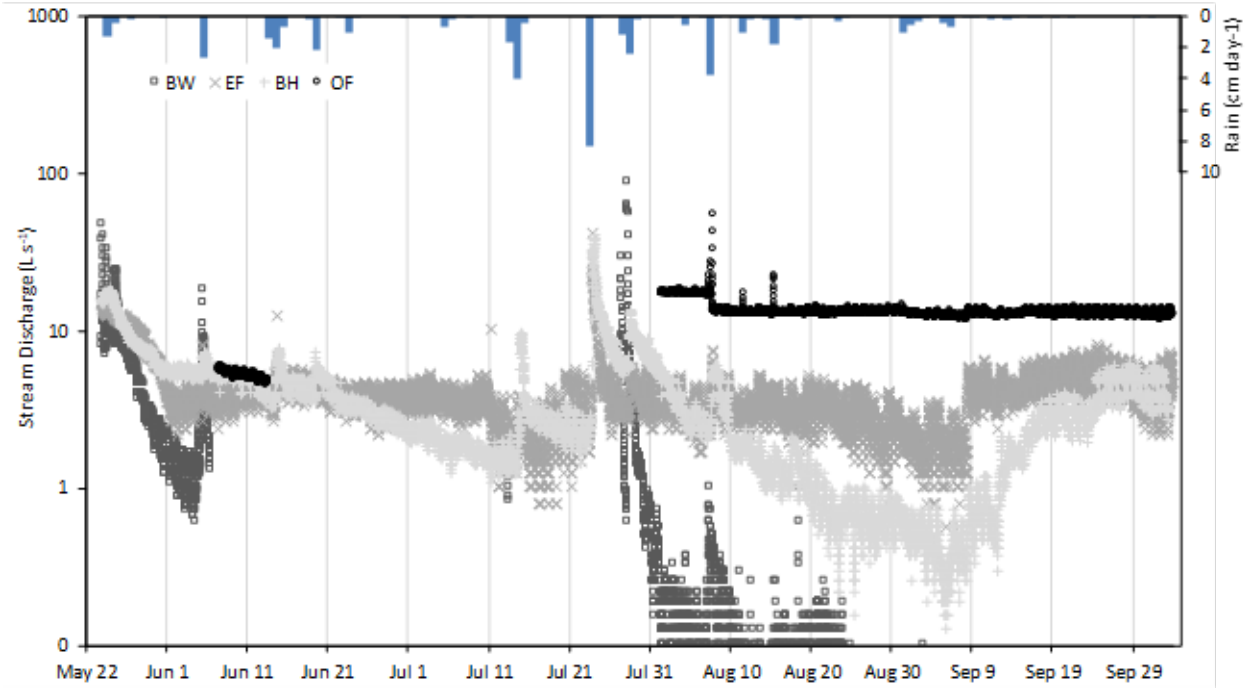

Figure D-2: Streamflow and Precipitation during Field Season

The data file from Bearwallow from 06/06/17 – 07/10/17 data file was corrupt. The Office Fill streamflow data is irregular because the streambed was unstable, such that the flume frequently was clogged or bypassed. The precipitation data shown is for Office Fill, End Fill, and Barton Hollow, which were all at the same mine.

Appendix E – Procedure for Scaling Time-Lapse Tomograms

The initial time-lapse inversion on each set of raw data from our ERI surveys with rainfall yielded tomograms with a change in conductivity color scale ranging from -100% (red) to 100% (blue) by default (AGI 2009). On many of these tomograms, the changes in conductivity were difficult to see because of the broad scale range.

The inversion also produced data files providing numerical values for the changes in conductivity that the tomograms display visually. We examined these files to determine the most extreme change in conductivity observed, i.e., the percent difference with the largest absolute value, whether an increase or decrease in conductivity. We then specified this most extreme value as the outer end of the scale for the time-lapse batch inversion tool, so that the changes in conductivity would be as visible as possible in the resulting images, and reran the inversion. For example, if the largest change in conductivity observed was by 50%, we reran the inversion to create final tomograms with a color scale showing from -50% (red) to 50% (blue) change in conductivity.

Appendix F – Borehole Field Setup Photographs


J. L. Sexton & Son

Appendix G – Soil Pit Excavation Field Setup Photographs

Office Fill


36.5


34

End Fill – General

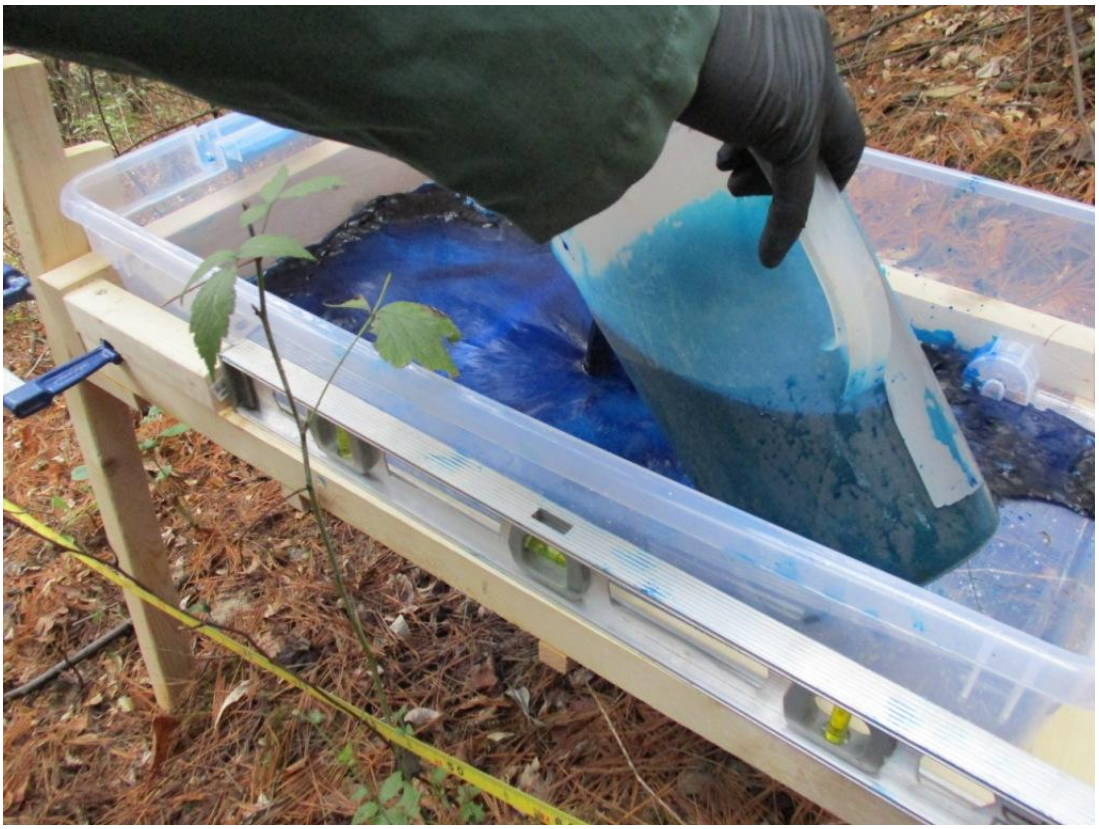

End Fill - Station 24

End Fill - Station 31

End Fill - Station 35

End Fill - Station 41